5-2001

Gloss Dynamics of Inkjet Printers

Amol G. Shirke

GLOSS DYNAMICS OF INKJET PRINTS

By

Amol G. Shirke

B.Tech. Indian Institute of Technology, 1996

A THESIS

Submitted in Partial Fulfillment of the

Requirements for the Degree of

Master of Science

(in Chemical Engineering)

The Graduate School

The University of Maine

May, 2001

Advisory Committee:

Douglas W. Bousfield, Professor of Chemical Engineering,

Advisor

Adriaan van Heiningen, Ober Chair and Professor of Chemical

Engineering

Yang Xiang, Research Engineer

GLOSS DYNAMICS OF INKJET PRINTS

By Amol G. Shirke

Thesis Advisor: Dr. Douglas W. Bousfield

An Abstract of the Thesis Presented
in Partial Fulfillment of the Requirements for the
Degree of Master of Science
(in Chemical Engineering)
May, 2001

Inkjet printing is a popular non-impact technology with widespread use in home and office applications. The basic principle involves propelling ink drops of different colors on a substrate. High quality images, near photographic quality, are now possible.

The gloss of the printed substrate is an important quality attribute. Printed gloss depends on a number of characteristics of the media and the ink, but a good fundamental understanding is not available in the literature. The dependence of the gloss on the media and ink characteristics is reported in this work. The experimental results are compared with values predicted by a mathematical model.

The dynamic post-printing gloss was studied with a specially constructed apparatus, which measured the laser reflectance of the printed surface within 40 ms after drop impact. Both pigmented and dye-based inks are used with rapidly absorbing porous media and swelling polymer-coated media.

Various properties of the media such as surface roughness, ink absorption rates, pore size distribution, oil absorption capacity, wettability, and gloss were

characterized along with ink properties like surface tension, viscosity, and filtercake resistance or the "filtercake" forming ability of the pigmented inks.

The model and experimental results show that the gloss of dye-based inks on porous media depends on the media roughness. Gloss on swellable media depends on the roughness of the wet swollen polymer coating. The gloss of pigmented inks on porous media is determined by the ink pigment size and the dry media gloss. The gloss on swellable media is determined by ink pigment size and the wet roughness. The model predictions compare well to experiments for a wide range of parameters.

ACKNOWLEDGEMENTS

The author wishes to express his deep gratitude to his advisor Prof. Douglas W. Bousfield for his boundless support, encouragement, and patience during the course of this work. Special thanks are also due to Drs. Nils Miller and Amiya Chatterjee at Hewlett-Packard, and the committee members Prof. Adriaan van Heiningen, and Dr. Yang Xiang for their valuable time and advice.

The author wishes to thank Prof. John C. Hassler for his indispensable help in building and programming the experimental apparatus.

Thanks are also due to Dr. Yang Xiang, and Manish Giri for their help with the experiments, and valuable discussions, and to Martine Bouchon for correcting my numerous mistakes.

The research was funded by Hewlett-Packard at the University of Maine.

A final word of appreciation goes to the author's family for their love, support and encouragement, and to the grace of the Almighty without which this work would not have come to completion.

Table of Contents

List of Tables

List of Figures

Chapter 1: Introduction

Inkjet printing has become an important printing technique in recent years due to the low cost of inkjet printers and their ability to accurately reproduce graphic color images on paper. In recent times, advances in inkjet technology have made it possible to print images with photographic quality. As a result, there is a demand for high gloss finishes, which entail specialized coatings [1]. The motivation for this project stems from the problems encountered in producing a high level of print gloss on glossy inkjet media.

The basic principle of inkjet printing involves propelling a drop of ink onto the paper. Inkjet technology is classified as drop on demand (DOD) or continuous depending on whether all the drops impact the substrate or not. In continuous inkjet, the ink contains charge generation additives and the fired drops are selectively charged and deflected onto the substrate using an electrical field [2]. Depending on the technique used to eject the ink drop, the DOD technology can be classified as thermal inkjet or piezo inkjet.

Thermal inkjet technology uses heat to create an expanding vapor bubble, which is used to propel the drops. Piezoelectric technology circumvents the use of heat by using a piezoelectric crystal, which is made to vibrate by an electric signal, thereby propelling the drop.

The inks used with continuous inkjets are not constrained by heat stability, and do not suffer from kogation or a buildup of ink residue inside the printhead due to the evaporation of the ink components [3].

The printed image is formed by using three basic colors- cyan, magenta, and yellow. The color gamut is realized by combining these three colors on the paper in various combinations. A separate reservoir for black ink is usually used for black prints, since a combination of the three basic colors does not produce a realistic black.

1.1 Factors affecting print quality

The non-impact nature of inkjet printing endows it with a unique set of print quality attributes. Some of the problems encountered in inkjet printing are bleeding, banding, dot spread, smearing, and fading.

Capillary diffusion into pores by wicking into unprinted areas causes bleeding. Inter-color bleed, which is the mixing of adjacent colors, is also a related printing defect. Misfiring nozzles in the printhead lead to light and dark patterns, called banding. Lateral spreading of the drops, leads to a larger dot size than intended, called dot gain. A printed sheet has to be adequately dry before the next printed sheet is stacked on top of it. This necessitates that the media have relatively low drying time to avoid smearing. Light fastness and water fastness, which can be defined as resistance to color loss due to exposure to atmospheric/ultraviolet radiation, and water, respectively, are also important requirements.

1.2 Media requirements

The colored image is formed by mixing the three primary colors on the media. Also, different gray levels are obtained by laying down different numbers of ink drops in a certain area, called halftoning [2]. The inkjet coating should, therefore, have adequate coat weight to absorb more than a single drop at the same location, at a reasonable rate of absorption. A key condition to high throughput is rapid absorption of the ink. This is achieved by either highly porous coatings with large void volumes or water-soluble polymeric coatings, which swell and absorb the ink [4].

Inkjet inks are typically water-based, and the base layer of the medium is sometimes reinforced by a backing layer to prevent curling effects due to humidity or temperature changes. One of the mechanisms used to dry inkjet prints is evaporative drying in which hot air is forced over the printed medium, to allow for high throughput printing rates, which exposes the medium to the effects of curl [5]. The printed medium also needs to be water-resistant, to prevent dissolution of the prints by water.

1.3 Ink requirements

Inkjet inks have to satisfy the primary constraints posed by both, the firing process, and the level of print quality. Inks used in piezo technology are not constrained by the effects of high temperature, which is necessary to fire drops in thermal inkjet printers. Two types of inks are primarily used- pigmented, and dye-based. Dye-based inks contain dye molecules, which are soluble in the ink carrier liquid and are uniformly dispersed throughout the ink. Pigmented inks on the

other hand contain water-insoluble pigments, which are dispersed as a stable colloidal suspension [6].

The inks used in inkjet printing are fluid to ease the jetting process, and have viscosities from 1 to 10 mPas, with continuous-inkjet inks at the lower end of the range. This is necessary since the diameters of the printhead nozzles are typically in the range of 10-30 microns, and the drop volume around 10-120 picoliters [7] in currently available printers, and depends on the type and resolution of the printer. Continuous inkjet printers use drop volumes around 10 picoliters, and frequencies up to a million drops per second [2], while thermal DOD printers reach frequencies up to 12000 drops per second [7].

The inks have to be able to wet the medium with minimal delay, and with controlled spreading to have good dot definition. The lightfastness and waterfastness of prints is also an important requirement for outdoor applications such as billboards and posters, where the printed medium has to be able to withstand the effects of weathering and sunlight.

The dye-based inks undergo oxidative or reductive fading in ultraviolet environments, and when exposed to the atmosphere [8], while providing a wider color gamut than pigments. This is due to the fact that dyes are monomolecular, with large surface areas, while pigments are molecular aggregates, with only 10 % of the surface molecules contributing to the optical effects.

DOD inks typically contain water as the main component (60-90 % concentration). The other components are dye or pigment (<10%), water-soluble solvent as a humectant and for viscosity control, a surfactant to aid wetting,

biocide to prevent bacterial growth, a buffer to control the ink pH, and other additives like defoamers, solubilizers, and chelating agents. Continuous inkjet inks have lower viscosities, due to their high firing rates, and charge generation additives to enhance the charge generating capability of the ink [2]. The dye molecules penetrate the coating along with the carrier liquid, and are immobilized near the surface, while the pigments are deposited on the surface when the ink carrier is absorbed by the medium.

1.4 Media composition

The types of inkjet media commercially available are a) surface sized paper, b) matte coated paper, and, c) glossy coated paper. Surface sized paper is uncoated, and produces medium quality of prints, while matte paper gives a better output with vibrant colors. Coated glossy paper gives the highest photographic quality color output [4].

The prevalent types of glossy inkjet media are cast-coated, swelling, and microporous [9]. Cast-coated media suffers from drawbacks such as low optical density, gloss and the cockling or deformation effects of its paper base. Swelling or resin rich and microporous media sometimes have the base paper covered by a polyethylene layer that is impermeable to ink.

The resin rich coatings typically contain water-swelling polymers such as gelatin, poly-vinylcohol (PVOH), and poly-pyrrolidone (PVP). Another resin combination is colloidal alumina dispersed in a hydropropylcellulose/PVOH matrix. The resin coatings absorb inks by a swelling mechanism, by which the polymer swells and absorbs the ink [1].

Microporous media coatings are formulated above the critical pigment volume concentration (CPVC), and are composed primarily of amorphous silica and/or alumina, with a polymeric binder like PVOH [4]. The pigment volume concentration is defined as the ratio of the volume of pigments to the sum of the volumes of the pigment and binder in the coating. "The CPVC is the point at which just sufficient binder is present to completely fill the voids left between particles in a pigment-binder system. It represents the densest degree of packing of the pigment particles commensurate with the degree of dispersion in the system" [9]. The CPVC is of importance since the physical and optical properties of coatings undergo a dramatic change above the CPVC.

The amount of binder used must be low to maintain the microporous void volume. Also, a non-swelling polymer should be used so as not to hinder the absorption process. The mechanism of capillary absorption is used to absorb the ink in the highly porous network [1].

1.5 Ink-media interactions

The processes, which occur at the ink-media interface after the ink has been deposited, control the ultimate image quality. The events that occur directly after the ink drop has been fired are- impact on the substrate, wetting, and absorption.

On impact with a non-absorbent substrate, the drop spreads radially into a pancake shape. The rate of spreading is controlled by the inertia of the drop and the viscous effects [10], which work in opposition. The drop reaches its maximum flat diameter when the kinetic energy is dissipated, and then assumes an

equilibrium shape when the retracting surface tension forces balance the spreading. On an absorbent substrate, the rate of absorption may be a factor. Also, the initial drop impact is a solid-liquid interfacial interaction, whereas the subsequent interactions may involve various combinations of interfacial forces depending on whether the drop hits a pre-wetted surface, or another drop. The time required for the kinetic energy dissipation of low-velocity drops (~1m/s) is a few milliseconds on dry or pre-wetted paper surfaces [11].

1.5.1 Wetting

A drop of liquid placed on a solid usually assumes an equilibrium shape, when the interfacial forces balance each other. Figure 1.1 illustrates this concept.

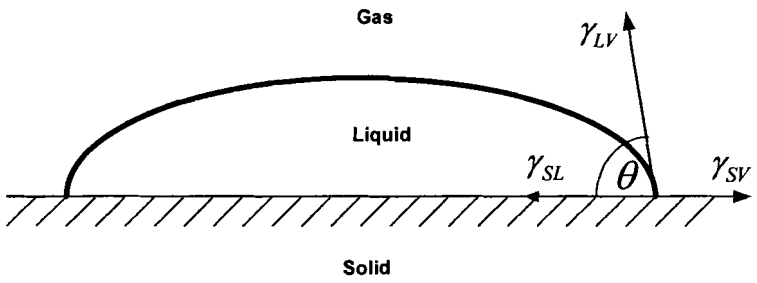

Figure 1.1 Idealized contact angle on smooth solid surface

As can be seen, the angle made by the gas-liquid interface at the solid boundary, measured from inside the liquid phase, is called the contact angle (θ). The force balance is represented by the Young and Dupre equation [12],

$$\gamma_{LV}\cos\theta = \gamma_{SV} - \gamma_{SL} \tag{1.1}$$

where γ_{lv} is the liquid-vapor interfacial tension acting along the perimeter of the drop, with S, L, and V denoting the solid, liquid, and vapor phases respectively. The above equation represents the horizontal force balance on an idealized smooth surface. For rough surfaces, an additional factor β (>1) is introduced to account for the underestimated surface area in eq. (1.1). The equation becomes,

$$\beta\gamma_{LV}\cos\theta = \gamma_{SV} - \gamma_{SL} \tag{1.2}$$

In case of the surface being chemically heterogeneous, additional factors are introduced [13]. Assuming that the surface is composed of two heterogeneous fractions of types 1 and 2, the equation can be written as

$$\beta\gamma_{LV}\cos\theta = f_1(\gamma_{S1V} - \gamma_{S1L}) + f_2(\gamma_{S2V} - \gamma_{S2L}) \tag{1.3}$$

where

$$f_1 + f_2 = 1$$

A contact angle greater than 90^0 implies a non-wetting liquid, while a value of zero means complete wetting. When a solid surface has a roughness factor r, the ratio of actual to projected area, the solid-gas and solid-liquid interfacial free energies per projected unit area are increased by a factor of r, assuming unaffected interfacial tensions. The equilibrium contact angle ϕ_{eq} is then given by

$$\cos\phi_{eq} = r\cos\theta_{eq} \tag{1.4}$$

which is called Wenzel's equation, with θ_{eq} as the Young contact angle, and is valid when the size of the roughness structure is much smaller than the contact radius of a liquid drop [14]. Figure 1.2 shows the cross-section of a sessile drop on a sinusoidal rough surface.

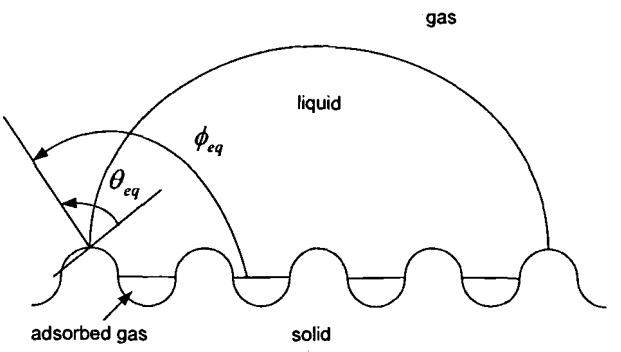

Figure 1.2 Apparent contact angle on a sinusoidal rough surface

Another parameter to measure the wettability of a surface is the spreading coefficient $S_{L/S(V)}$. A positive value of the spreading coefficient $S_{L/S(V)}$, where

$$S_{L/S(V)} = \gamma_{SV} - \gamma_{LV} - \gamma_{SL} \tag{1.5}$$

implies that the liquid freely spreads over, and wets the solid, while a negative value means that the liquid does not spread on the solid. The solid-liquid interfacial tension can be determined from the relation due to Rayleigh, and later Good et al. [15], as

$$\gamma_{SL} = \gamma_{SV} + \gamma_{LV} - 2\sqrt{\gamma_{SV}\gamma_{LV}} \tag{1.6}$$

Combining Eqs. (1.1) and (1.5) gives

$$\gamma_S = \frac{1}{4}\gamma_{LV}(1+\cos\theta)^2$$

where γ_s is the same as γ_{sv} if adsorption of the vapor on the solid is neglected. Neumann et al. [15], proposed an equation of state, Eq (1.7), which in conjunction with the Young-Dupre equation, can be used to determine the interfacial tensions.

$$\gamma_{SL} = \gamma_{LV} + \gamma_{SV} - 2\sqrt{\gamma_{SV}\gamma_{LV}}\, e^{-\beta(\gamma_{LV}-\gamma_{SV})^2} \tag{1.7}$$

where $\beta = 0.000115\ (\text{m2/mJ})^2$

The spreading coefficient can thus be calculated once the interfacial tensions are known.

1.5.2 Absorption

The process of liquid absorption by porous media can be modeled as the spontaneous penetration into a capillary due to surface tension, using the Lucas-Washburn theory [10].

Assuming that the meniscus is a section of a spherical surface that intersects the capillary at a finite contact angle θ_d, the pressure difference across the interface can be written as

$$\Delta P = \frac{2\sigma}{R}\cos\theta_d \tag{1.8}$$

where σ is the surface tension of the liquid, and R is the capillary radius. The effect of gravity is neglected in the above equation. Assuming a Newtonian low-velocity flow, the Poiseuille equation gives the average velocity of the liquid rising in the capillary as

$$\frac{dx}{dt} = \frac{R^2\Delta P}{8\mu x} \tag{1.9}$$

where x is the length of the capillary that is wetted, and μ is the liquid viscosity. Integrating Eq.(1.9) gives,

$$\frac{L}{R} = \left(\frac{t\sigma\cos\theta_d}{2\mu R}\right)^{1/2} \tag{1.10}$$

where L is the length of the capillary wetted in time t. Middleman [10] gives an equation incorporating the effects of gravity in the form

$$T = -H^2[\frac{X}{H} + \ln(1 - \frac{X}{H})] \tag{1.11}$$

where

$$T = \frac{t4\sigma\cos\theta_d}{\mu R}$$

$$X = \frac{4x}{R} \text{ , and } H = \frac{8\sigma\cos\theta_d}{gR^2\rho}$$

The Lucas-Washburn equation, however, applies to cylindrical capillaries, and does not always apply to penetration of aqueous inks into paper. The Lucas-Washburn equation also does not take into account the fiber swelling and pore size distribution effects [16]. It is also not possible to separate the effects of r and $\cos(\theta_d)$ from Eq.(1.10).The effects of capillary prewetting and the unknown dependence of the dynamic contact angle on the rate of rise are also important issues. Joos et al. have presented an experimental relationship in the form

$$\cos\theta_d = \cos\theta_c - 2(1+\cos\theta_c)Ca^{1/2}$$

where θ_c is the equilibrium contact angle and Ca is the capillary number defined as

$Ca = \frac{\mu U}{\sigma}$ and $U = \frac{dx}{dt}$ is the average velocity of the liquid rising in the capillary [10].

Marmur recast the Lucas-Washburn equation, and adapted it to a capillary assembly model [17], which assumes a pore size distribution, but with the

advantages of being able to separate the effects of r and $\cos\theta_d$. The Lucas-Washburn equation is rewritten as

$$At = -Bh - \ln(1 - Bh) \tag{1.12}$$

where

$$A = \frac{\rho^2 g^2 r^3}{16\sigma\mu\cos\theta}$$

and $B = \frac{\rho\ g\ r}{2\sigma\cos\theta}$, with ρ as the density difference between the liquid and fluid.

Eq. (1.12) when written as an infinite series of dimensionless terms, is

$$1 = \frac{1}{2}\frac{B^2h^2}{At} + \frac{1}{3}\frac{B^3h^3}{At} + \frac{1}{4}\frac{B^4h^4}{At} + \ldots \tag{1.13}$$

useful in separating the effects of r and cos θ.

1.6 Factors affecting gloss

Gloss is an important optical parameter in evaluation of print quality. The psycho-physiological sensation of gloss is a measure of the surface reflection of light in the specular direction. In contrast, a surface reflecting light in all directions, produces a sensation of a "non-shiny" or matte surface.

The gloss is the portion of light reflected in the specular direction at an angle equal to the incident angle. High gloss implies a higher fraction of incident light being reflected in the specular direction. Scattering reduces the amount of specularly reflected light, thus reducing gloss. Figure 1.3 illustrates the concept of diffuse and specular reflection, while Figure 1.4 shows the interaction of light with the paper and ink layers.

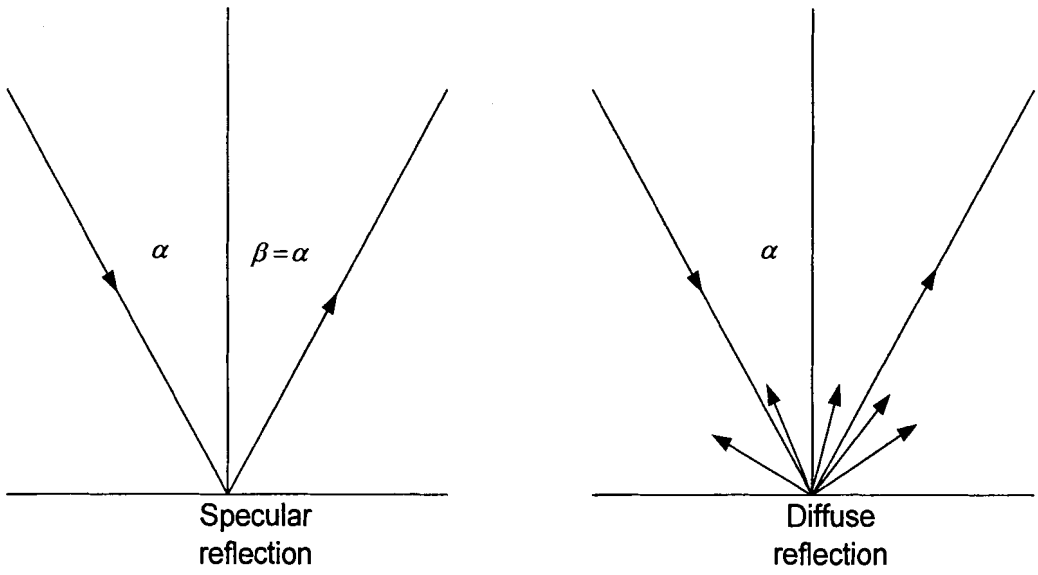

Figure 1.3 Specular (mirror-like) and diffuse reflection (scattering) [2]

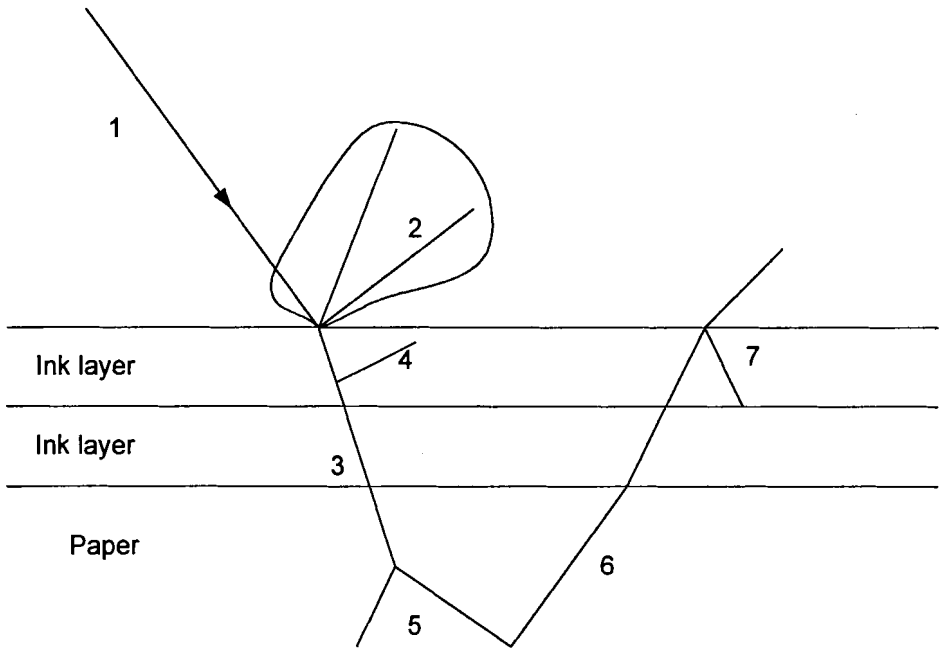

Figure 1.4 The phenomena of light interaction with a print [2]

1) Incident light beam
2) Surface reflection distribution
3) Light traveling in the ink layer (absorption)
4) Scattering of light in the ink layer caused by ink opacity
5) Scattering of light in the paper causes optical spreading
6) Reflection of light from the paper
7) Internal surface reflection

The first interaction between the image and the light is the surface reflection from the ink-air interface. Surface reflection from prints has the same spectral composition as the incident light. The unreflected light undergoes refraction in the ink layers. The refractive indices of the various layers determine the amount of surface reflection that can occur. A high refractive index implies a high magnitude of the surface reflected light at any given angle of reflectance. In the ink layer, depending on the color of ink, spectrally selective light absorption occurs. The refractive indices of inks and paper are approximately the same and hence there is little optical interface between them, which can cause significant surface reflection.

In the paper substrate, light scattering takes place. Scattering is the traveling of light in all directions. A high degree of scattering means that the light penetrates to a smaller depth before backscattering. Scattering also causes random polarization and causes the light to travel sideways into the paper, which causes optical spreading, or an enlarged printed spot. Light scattering and absorption

determine the paper opacity. The combined effect of scattering and absorption is that some light reflects from the paper and refracts into the ink layers. At the interface between the topmost ink layer and air, some light undergoes internal surface reflection back into the ink layers. Multiple reflection causes a reduction of light intensity.

In spite of several studies on ink and coating gloss development, the mechanisms controlling the process are not established [18]. A study of the dependence of ink gloss development on ink absorption revealed that immediately after the nip printing event, the rate of leveling of the ink layer defects, their magnitudes, the printing speed and ink film thickness affected the gloss development. It was found that print gloss increased over time as the defects leveled out, with the larger defects, which were produced by thick inks, leveling slowly [19]. Another study found that the coating absorbency, which affects the ink film contribution to gloss, to be strongly dependent on coating pigment size, pigment surface area, and binder content. The sizes of the coating pores were found to be proportional to the pigment pore diameters, while the number of pores was inversely dependent on the binder content. The smaller pigments produced narrower pores; faster ink setting, and lower print gloss. It was concluded that very small coating pigments may produce high paper gloss but low print gloss [20]. A study of various coating structures for a correlation with high offset-print gloss revealed that high print gloss could be obtained on coatings with small pores on the surface, with large internal pore volume [21].

Gloss can be measured by commercial glossmeters with different angles of incidence and corresponding angles of acceptance. The 100% gloss value is usually assigned to a reference black glass.

In an attempt to correlate the gloss uniformity of offset-printed paper samples with the local macro and microroughness, it was found that roughness was insufficient in predicting the local reflectance and a nonlinear correlation was obtained [22].

The dependence of specular reflection on the incident angle, wavelength, and surface roughness can be seen in the following equation

$$\frac{I}{I_o} = f(n,i)\exp[-(4\pi\sigma\cos i/\lambda)^2] \tag{1.14}$$

where I and I_o are the specularly reflected and incident light intensities, respectively, f(n,i) is the Fresnel coefficient of specular reflection as a function of refractive index n and angle of incident light i, σ the standard deviation of the surface roughness, and λ is the wavelength of incident light [23]. The TAPPI 75° gloss of coatings can be related to the same parameters as follows

$$\text{TAPPI } 75^\circ \text{ gloss} = 384.6\, f(n,75^\circ)\exp -(4\pi\sigma \cos 75^\circ/0.55)^2 \tag{1.15}$$

For paper coatings with similar refractive indices, the TAPPI gloss can be thus seen to be mainly dependent on the surface roughness. The effect of pigment particle sizes, binder level, drying conditions of binder films, and calendering on coating gloss was found to be attributable to their effects on the roughness. The addition of small pigments increases the coating gloss of monodispersed pigments. The gloss of coated papers also increases with increasing coat weight,

but levels off at high coating weights. Supercalendering helps flatten the coating surface, but cannot remove microscopic surface irregularities [24].

This study was aimed at determining the various factors which would affect the gloss development, and the final print gloss of ink jet substrates, which have not been extensively investigated, and present rather new problems due to the unique coating and ink composition, and the non-impact nature of the printing method.

Chapter 2: Media and Ink Characterization

A series of inkjet media and inks were characterized with standard and novel methods to determine the key parameters controlling the ink-media interaction. Some of the tests included surface profilometry using an atomic force microscope and a stylus probe, silicon oil and water absorption tests, static and dynamic contact angles with water, and mercury porosimetry. The test descriptions, theoretical aspects, and the results will be described in this chapter.

2.1 Media specifications

Two broad categories of media were used for the study:

1) glossy resin rich media with a water-soluble polymeric coating, which swells and absorbs the ink, and
2) microporous, non-swellable media with rapid absorption properties. Commercially available glossy photographic media manufactured by Hewlett Packard and Epson were used as the test samples. The media will be specified by the following notation:
    1) MS1 - (media, swellable), film base
    2) MS2 - paper base
    3) MS3 - paper base
    4) MS4 - paper base
    5) MP1 - (media, porous), film base
    6) MP2 - film base

2.2 Atomic Force Microscopy

Atomic force microscopy was used to study the surface profile and features of the media to look at the level of microroughness involved. The atomic force microscope (AFM) belongs to the class of scanning proximity probe microscopes. The primary component of the AFM is the optical lever, which is connected to a probing tip or cantilever. The cantilever is made to vibrate (depending on the mode of operation) and a laser beam is made to reflect off the lever, which is connected to the cantilever. Figure 2.1 illustrates the basic principle of the optical lever.

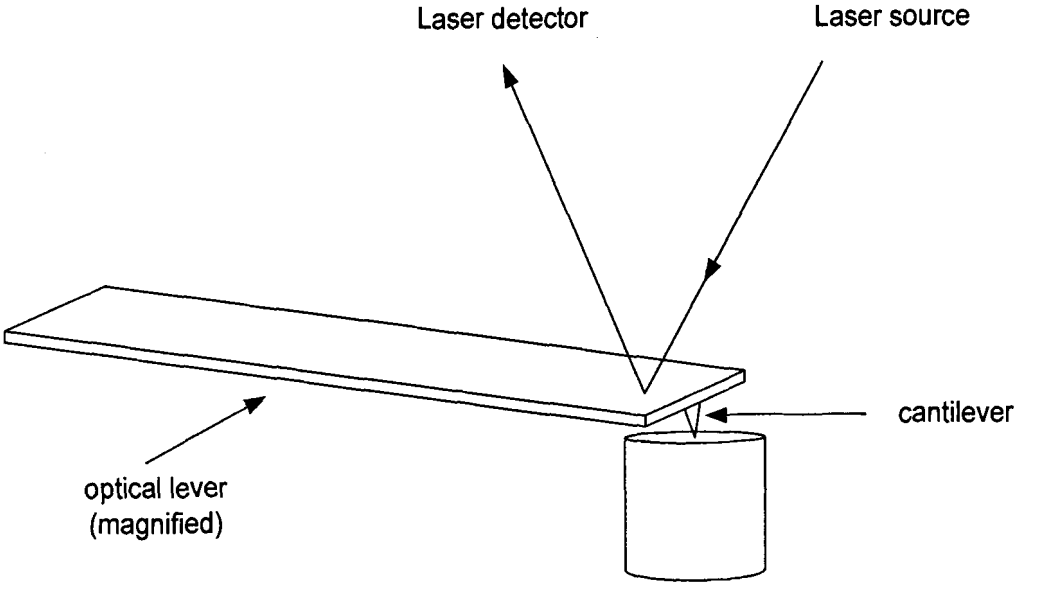

Figure 2.1 AFM operating principle

The signal from a position sensitive laser-detector helps create the topographical map of the surface. The geometry and dimensions of two cantilevers are shown in Figure 2.2.

Figure 2.2 AFM cantilever geometries

The relevant modes of operation of the AFM are the non-contact (NC) and intermittent contact (IC) mode, both of which use a vibrating cantilever held tens to hundreds of angstroms above the sample surface. The cantilever tip either makes no contact with the sample (NC mode) or does so only at the lowest point in its vibration cycle (IC mode). Since there is little or no contact between the tip and the surface, this method can be called non-intrusive, and can be effectively used with samples like soft polymers or biological materials, which can be damaged by the boron-nitride tip [25].

In the NC mode, the cantilever tip is held about 50 to 100 $\mathring{A}$ above the sample surface during a scan. It is vibrated at a constant frequency near its mechanical resonant frequency (typically 100-400 kHz), with an amplitude of a few tens of angstroms. As the tip is scanned above the surface, the cantilever vibration amplitude changes in response to force gradients that vary with the tip-to-sample spacing. An image representing the surface topography is obtained by monitoring these changes in vibration amplitude.

In the IC mode, the cantilever tip is brought closer to the sample, with a higher vibration amplitude so that at the bottom of its travel path it just hits the sample. Imaging large scan sizes (greater than a few μm) and surface features (greater than a few hundred nm) is best accomplished by using the IC mode. NC mode usage does not suffer from the effects of tip or sample degradation, which sometimes occur after numerous scans in the contact mode.

The AFM was an Autoprobe M5 model, manufactured by Park Scientific Instruments. The x-y scan ranges possible (horizontal movement) were greater than 90 μm, with a z or vertical range of 7.5 μm. The x-y and z scanner resolutions were 18 $\mathring{A}$ and 1.2 $\mathring{A}$ respectively. The media samples were tested using the contact mode, since extremely soft materials were not involved.

The samples were tested at room temperature. The humidity in the room was not controlled. Figure 2.3 shows the results of the AFM scans. The swellable medium MS3 shows the highest roughness, followed by one of the porous media, MP2.

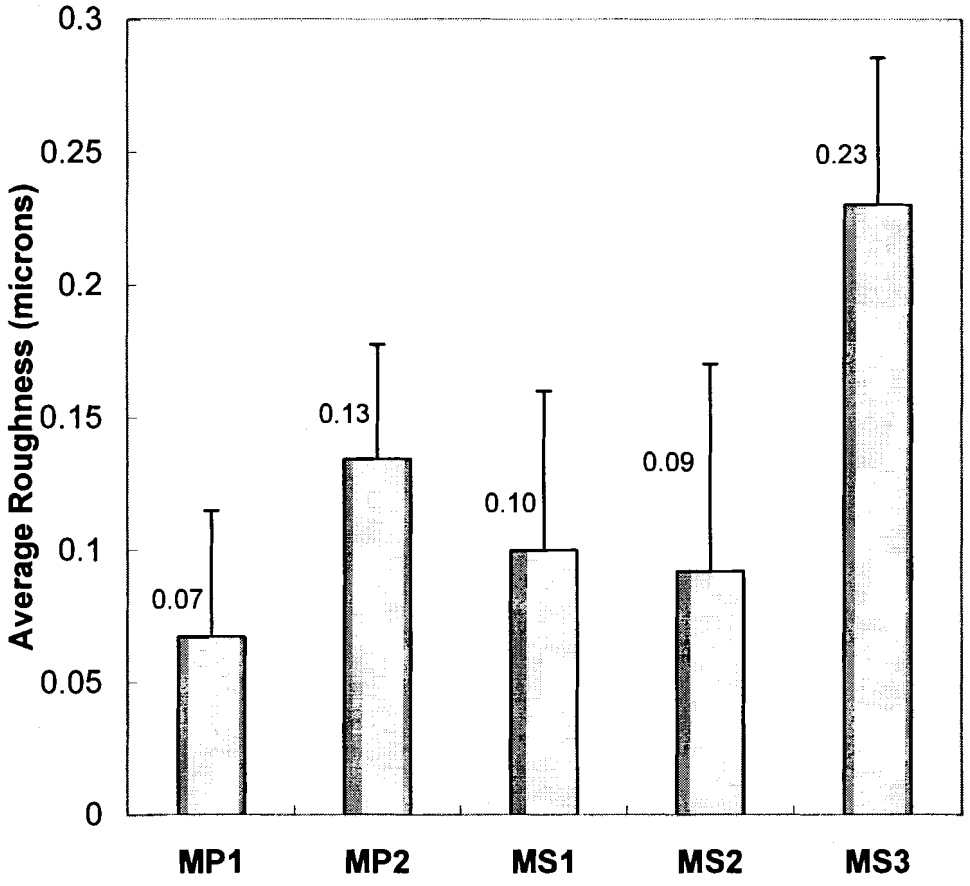

Figure 2.3 Average roughness measured by the AFM

2.3 Stylus profilometry

The AFM is best suited for profilometry at a relatively finer level of resolution. The stylus profilometer was used to obtain an idea of the features involved at a "macroscopic scale". The basic operating principle involves the motion of a stylus over a surface at a fixed imposed vertical force. The surface profile is then obtained from the actual path followed by the stylus. The instrument used for the tests was an Alpha-Step 200 manufactured by Tencor Instruments [26].

The available scan lengths were 80, 400, 2000 and 10000 μm, with scan times of 8 and 40 seconds. The highest resolution possible was 5 $\mathring{A}$ with the upper limit of measurement being 320 μm, in the vertical direction. The horizontal resolution was 400 $\mathring{A}$, with upto 2000 data points sampled on every scan. The stylus can be modeled as a 60

degree cone rounded to a spherical tip of 12 μm, as can be seen in Figure 2.4 The limitation posed by the size and geometry of the stylus on the measurable size of a groove is also illustrated. The dotted line shows the actual path followed during a scan, which differs from the ideal path, for the above reason. Another controllable parameter is the stylus force, which is the vertically applied force on the sample during measurement. A maximum of 25 mg is available with the Alphastep 200.

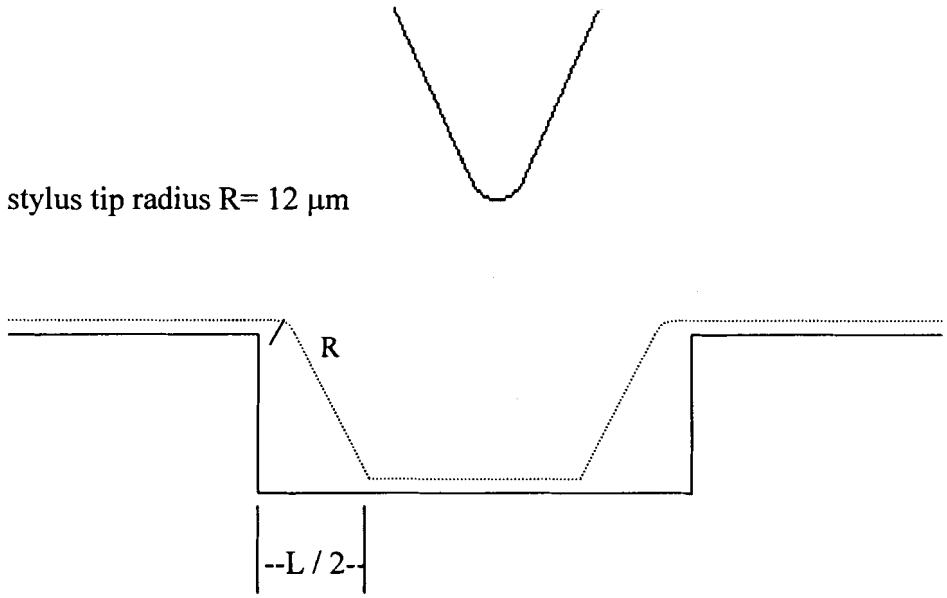

L: Apparent loss of groove width

Figure 2.4 Stylus tip geometry and its effects on measurement

A scan length of 10000 μm, a scan time of 40 seconds, and a force of 7 mg were used for the measurements. The highest length was used, with a view to getting a macroscopic profile of the samples, as opposed to that possible with an AFM. The stylus is easily capable of etching a path on coated paper, and hence a low magnitude of force was used. A lower force entails the risk of the stylus losing contact with the sample during the scan.

The profilometer provides an analysis of four important surface characteristics, such as the average height, the difference between the highest and lowest points, the average roughness, and the cross-sectional area. The arithmetic average roughness (Ra) is calculated as follows

$$Ra = \frac{\sum_{i=1}^{n} |y_i|}{n}$$

where the distances are measured from the centerline as shown in Figure 2.5

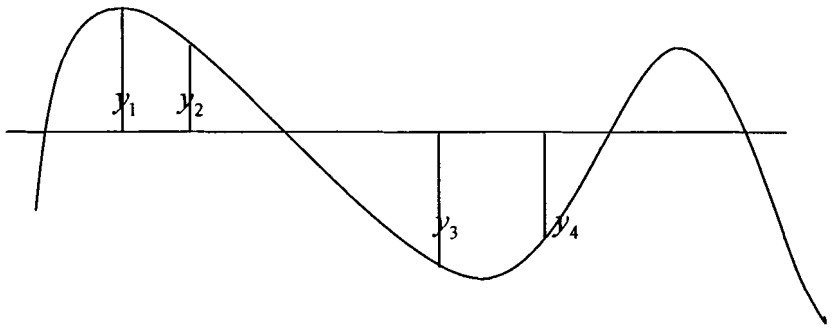

Figure 2.5 Measurement of roughness with the stylus profilometer

2.3.1 Roughness calculation methods

A real three dimensional surface, described by height z over an x-y plane requires a huge amount of information to completely describe it. Hence, the complex profile information is converted into a single number, which is easy to understand and compare using standard mathematical operations. This section describes some of the commonly used definitions of roughness.

A simple way of obtaining a roughness value for a one-dimensional profile z(x), is to calculate the average value of z(x) over distance L, as shown below.

$$\bar{z} = \lim_{L\to\infty} \frac{1}{L} \int_0^L z(x)dx \qquad (2.1)$$

The surface z(x) = $\bar{z}$ would be considered perfectly smooth. Roughness is defined in terms of deviations from the mean value. The arithmetic average roughness σ_a or R_a is given by

$$\sigma_a = \lim_{L\to\infty} \frac{1}{L} \int_0^L \left| z(x) - \bar{z} \right| dx \tag{2.2}$$

Another surface-height average is the root-mean square (rms) roughness σ or R_q, which is also defined in terms of surface-height deviations from the mean surface.

$$\sigma = \{\lim_{L\to\infty} \frac{1}{L} \int_0^L [z(x) - \bar{z}]^2 dx\}^{1/2}\} \tag{2.3}$$

The two values σ and σ_a are usually pretty close for most surfaces, and the following table gives an idea of the differences for idealized surfaces.

Table 2.1 Differences between average and rms roughness for idealized surfaces

Waveform z(x) (Peak to valley height: 2a)	σ_a	σ
Triangle	0.5a	0.58a
Sinusoid	0.64a	0.71a
Square wave	A	a
Circular cusp	0.51a	0.60a

An important point to be kept in mind is that the dependence of these calculations on height alone. Figure 2.6 shows two surfaces with different profile characteristics but the same roughness (σ or σ_a) [27].

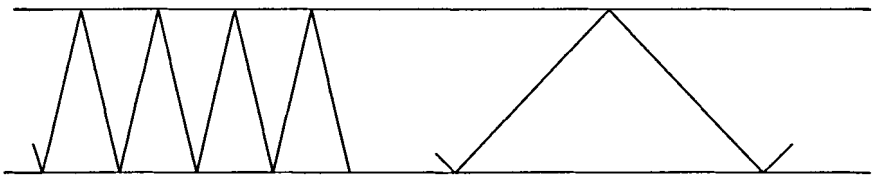

Figure 2.6 Two different surfaces with same roughness values

2.3.2 Stylus profilometry results

The trend in the stylus roughness is somewhat similar to that seen in the AFM results. MS3 is the roughest, followed by MP2, if MS4 is neglected. MS4 cannot be compared with the other samples with confidence, as it was obtained and tested at a later time. The conclusion that can be drawn from this observation is that though the AFM and stylus provide two levels of roughness analysis, the features at the macroscopic and microscopic scale are similar.

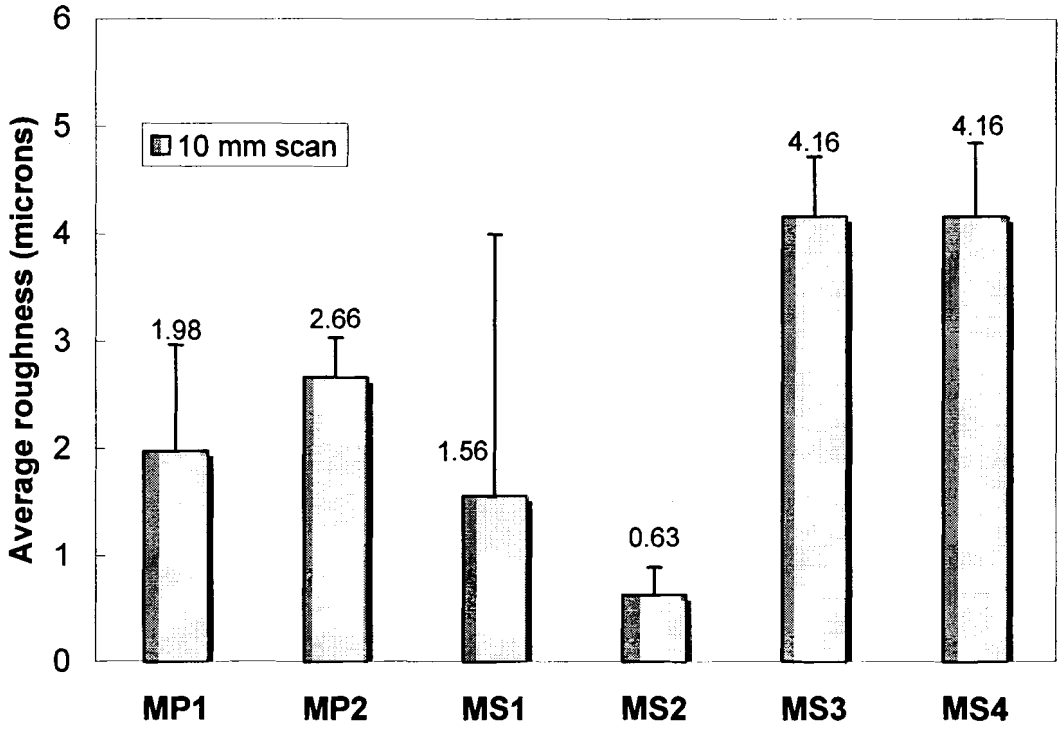

Figure 2.7 Comparison of stylus roughness of media samples

2.4 Silicone oil and water absorption results

The porosity of coatings can be measured by a gravimetric method in which the amount of silicon oil absorbed by the coating gives an idea of the volume of the voids occupied by air [28].

The void fraction, which is a measure of the coating porosity, is the ratio of the volume of displaceable air in the coating (in the voids accessible from the surface) to the sum of the volumes of the air and the coating components. Equation 2.1 defines the void fraction in terms of the silicon oil, which replaces the air in the original equation.

$$\text{Void fraction} = \frac{\frac{M_{oil}}{\rho_{oil}}}{\frac{M_{oil}}{\rho_{oil}} + \frac{M_{coating}}{\rho_{coating}}} \quad (2.1)$$

Where M and ρ stand for mass and density, respectively. The coating density can be determined from that of the individual components.

Three media samples of size 5 cm x 5 cm were weighed, applied silicone oil and allowed to soak for 15 minutes for complete penetration. The excess oil was wiped off, and the samples weighed again. To confirm the saturation, the oil was applied again, and wiped off, and the weights measured. Identical readings indicated the absence of excessive surface oil. The samples were allowed to soak for 5, 15, and 30 minutes to determine the time for saturation. Single values at 15 minutes are reported in Figure 2.5.

The water-absorption capacity of the samples was also measured in a similar fashion. The dry samples were weighed, and then covered with a layer of water for 15 minutes. The excess water was wiped off, and the samples were weighed again. Care had to be taken to prevent the base paper of some samples from absorbing the liquids. In addition, the resin-rich swellable media presented another problem of polymer dissolution in water. The excess water had to be carefully wiped off without removing the solubilized coating.

The porous and swellable media show comparable capacities, with the exception of MP1 and MS1, which lie at two extremes, as shown in Figure 2.8. The void fraction could not be calculated due to lack of coating weight data.

The water absorption results in Figure 2.9 do not show identical trends, but the medium MS2 shows a very high capacity. These results indicate that water must alter the pore structure of both MP1 and MP2. It is not surprising that the swellable coatings are able to take up more water than oil, because oil should not swell the polymer.

According to the Lucas-Washburn equation, a liquid of higher surface tension would have a higher penetration depth. Since the oil has a surface tension of the order of 20 dyne/cm, the water absorption for both media is much higher than the oil absorption. However MP1 absorbs more oil while MP2 absorbs more water, at saturation levels. This could be due to a higher surface-roughness volume of MP2, which could trap more liquid during the test, and water with a high surface tension would be considerably difficult to spread over the surface of the media.

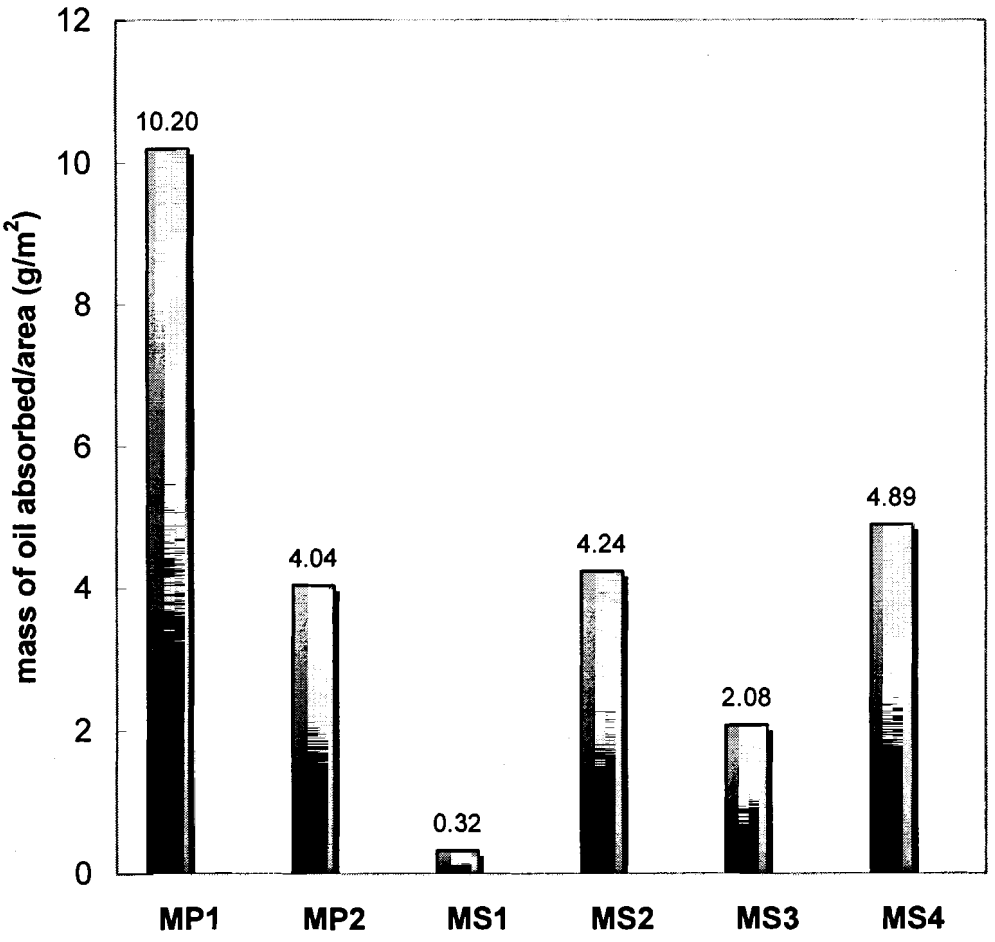

Figure 2.8 Silicone oil absorption capacity of different media

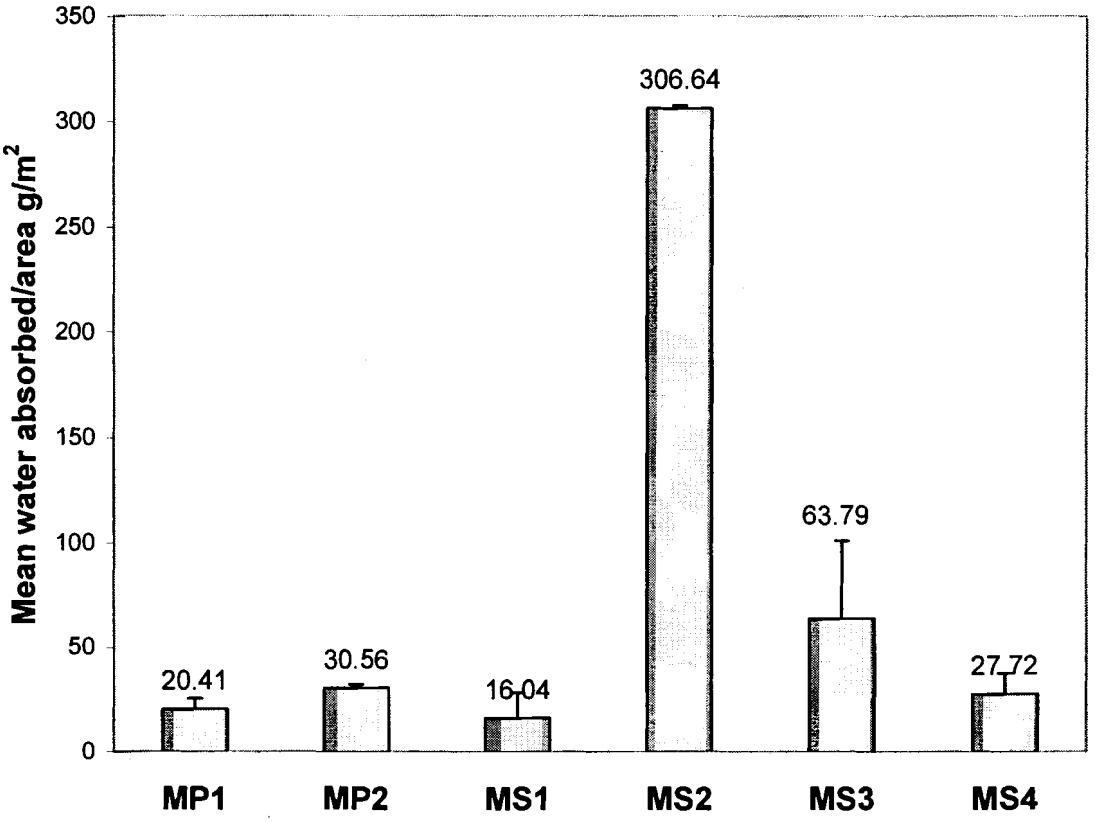

Figure 2.9 Water absorption capacity of different media

2.5 Static and dynamic contact angle results

To determine the wettability of the various media, the static contact angles of sessile drops of water were measured on the media samples. The theory of static contact angles has been discussed previously in the earlier sections. Drops of approximately 4 μL were deposited from a syringe held 2 mm above the media sample. The entire process was recorded by a CCD Sony video camera at frame

rates of 33 per second, and the images were analyzed with Image Pro Plus, an image processing software.

The advancing and receding contact angles are defined with respect to the drop profile assumed by a drop of liquid on an inclined surface. The larger angle θ_a is called the advancing angle and the smaller angle θ_r is called the receding angle. The angles are different due to various reasons, one of which is contamination. One of the methods of measuring contact angle or surface tension, the Wilhelmy plate method, can best describe the differences between two angles. The Wilhelmy plate method for measuring equilibrium contact angles involves measuring the weight of the meniscus entrained when a plate is immersed into a liquid. Figure 2.10 describes the basic principle behind the method.

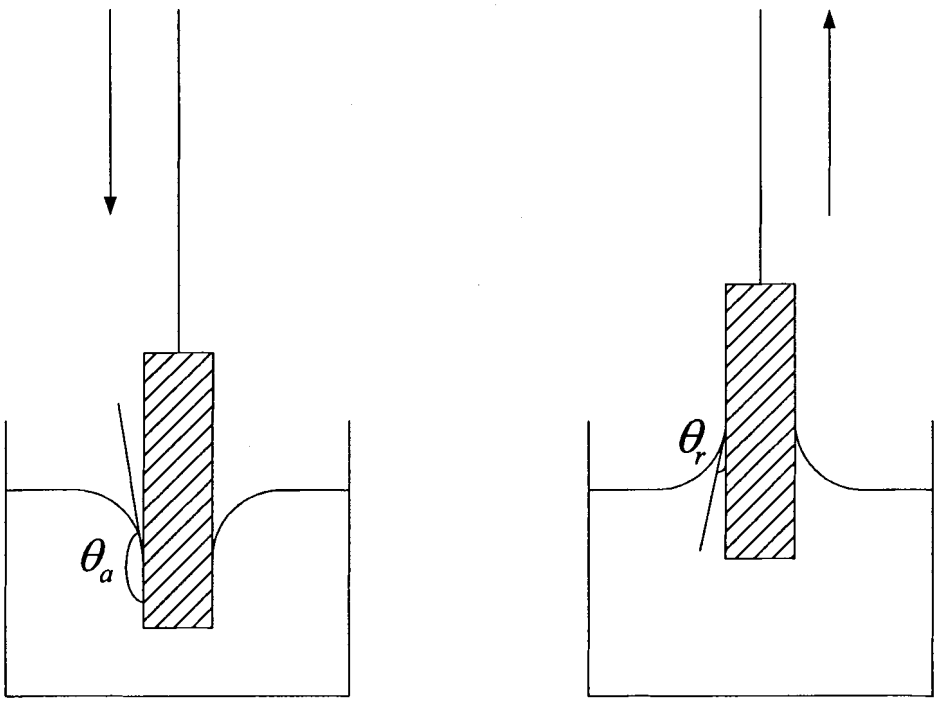

Figure 2.10 Wilhelmy plate method for static and dynamic contact angles

The upward force on the plate is balanced by the weight of the meniscus w, where

$$w = P\gamma\cos\theta \tag{2.2}$$

with P being the wetted perimeter of the plate and γ the surface tension of the liquid. When the plate is just touching the liquid surface in its equilibrium position, the above equation holds good, and it can be used to measure either the surface tension or the contact angle, the other parameter assumed to be known. When the plate is immersed to a depth d, the weight w is reduced by a buoyant force w', which can be assumed to be proportional to d. In other words,

$$w = P\gamma\cos\theta - kd \tag{2.3}$$

A plot of $P\gamma\cos\theta$ versus the immersion depth d, is expected to be linear, if the angle θ is constant during immersion and emersion. However, θ assumes two values, θ_a during immersion, and θ_r during emersion. This hysteresis behavior can be attributed to surface roughness, or the existence of various metastable energy states which are separated from each other by small energy barriers. The shape of the drop in each configuration corresponds to a metastable state from which it cannot go to a lower energy state without the use external forces. For example, vibrating the plate can help provide adequate energy to overcome the energy barrier and make the advancing and receding angles equal. The advancing contact angle usually represents the contact angle that would be obtained for a smooth surface corresponding to the energy of the low energy sites on the surface. Conversely, the receding contact angle corresponds to the angle assumed by the drop on a smooth surface with the energy of the low energy sites of the original surface.

The instrument used for the advancing and receding contact angles was a KSVSigma70 computer-controlled tensiometer. A Wilhelmy plate type of experiment was performed to measure the dynamic contact angles of water with the various substrates. A 1 cm x 3 cm strip of a sample was stuck back to back to another one of the same sample, since the substrates are single sided, and the edges were sealed with wax. The tensiometer consists of a sensitive electro-balance, which can measure forces from 0.25 μN to 25 μN [29].

For the tensiometer measurement, the Wilhelmy plate or sample is suspended from the stationary electro-balance hook. The liquid container is raised on a movable table at a predetermined speed. The samples were immersed and withdrawn (relatively) at a speed of 40 mm/min, which was the maximum allowed. The immersion depth was 8 mm below the liquid surface. Five readings were used in a cycle for each sample.

The results of the static and dynamic contact angle tests are shown in Figure 2.11. The static contact angles were measured at 1 second and 60 seconds after drop deposition. An average of 5 drops were used for the measurements. The dynamic contact angles were measured using a speed of 40 mm/min. The angles at 60 s are influenced by absorption and the receding contact angle.

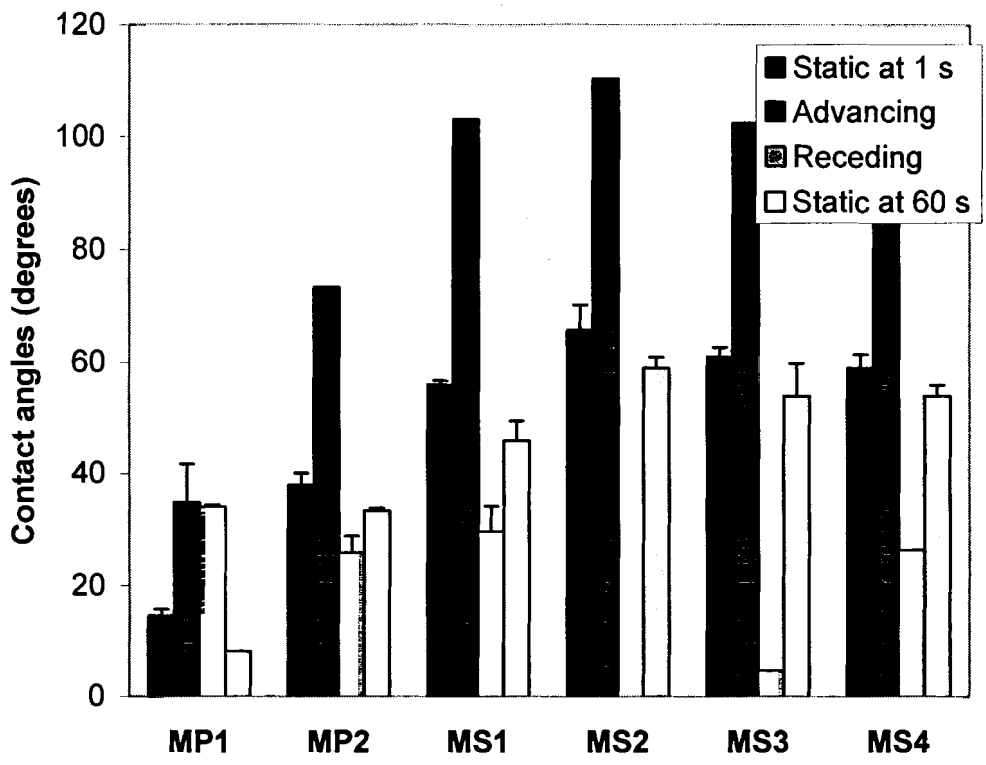

Figure 2.11 Static and dynamic contact angles of water

The swellable media show high values of advancing contact angles, which is consistent with the fact that they have low-energy polymer coatings. They also show higher static contact angles than the porous media, which also shows their low wettability characteristics. The high difference between the advancing and receding contact angles for the swellable media suggests a combination of high and low energy locations on the surface. However, it should be noted that the coating undergoes swelling during the test, and the liquid-solid interface is an expanding polymer matrix with the water molecules presenting wettable spots, and the polymer locations presenting low energy sites. Also, another interesting

observation is that the dynamic contact angles of MP1 are nearly identical, suggesting a composition with components having similar surface energies.

2.6 Mercury porosimetry

Mercury porosimetry uses the principle of pressurized capillary penetration by mercury to measure the pore size distribution of a substrate or powders. The instrument used was a Poresizer 9320 manufactured by Micromeritics. From the pressure versus intrusion data, the volume and pore size distribution are generated using the Young-Laplace equation, assuming cylindrical pores.

$$D = -(\frac{1}{P})4\gamma\cos\varphi \tag{2.4}$$

where D is the pore diameter, P is the applied pressure, γ the surface tension of mercury (485 dyne/cm), and φ the contact angle of mercury inside the pore, usually taken as 130^0.

Mercury does not wet most substances, and hence high pressure is required. The pressure needed for intrusion is inversely proportional to the pore size. Pressures ranging from 0.1 psia ($6.89x10^{-4}$ MPa) to 30000 psia (206.84 Mpa) are possible with the instrument [30].

The results of the mercury porosimetry tests carried out on the porous media, are shown in Table 2.2

Table 2.2 Summarized mercury porosimetry results

Intrusion Data Summary	MP1	MP2
Total Intrusion (Pore) Volume, mL Hg/g media	0.1472	0.206
Total Intrusion (Pore) Volume, mL Hg/m^2 media	25.38	37.60
Total Intrusion (Pore) Volume, g Hg/m^2 media	345.22	511.44
Total Pore Area, m^2/g	38.96	37.93
Average Pore Diameter, μm	0.0151	0.0214

The total intrusion pore volume (TIV) units represent the amount of mercury penetrating the pores, per gram of the sample. The porous media have a plastic base, and the coat weights are not known. The mercury can, therefore, penetrate only the coating. The total intrusion pore volume cannot, however be compared across media, due to the different coat weights involved. The other parameters are calculated based on the intrusion volume, assuming a cylindrical pore model. A comparison of the two media shows that on average, MP2 shows a higher pore volume and diameters. The TIV in terms of mass of mecury/area of the media shows a trend similar to that observed in the water absorption test. Another point to note is that percentage increase for MP2 over MP1 for both mercury and water is around 50%, indicating that the media are affected in a similar fashion in these two tests. The pore size distribution can be seen in Figure 2.12

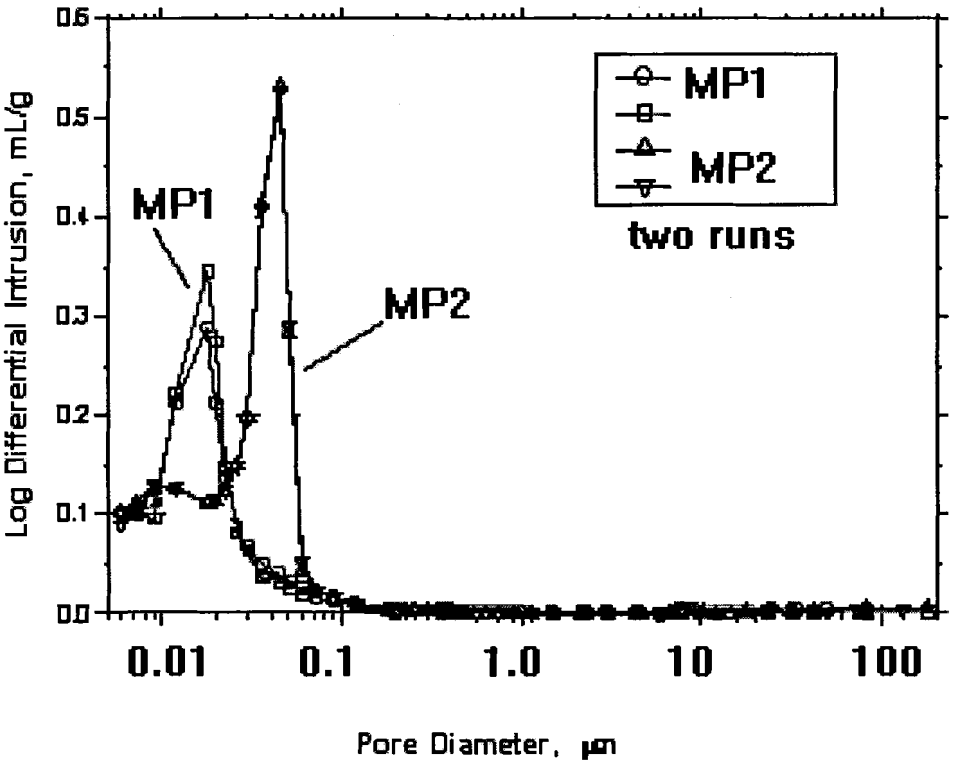

Figure 2.12 Pore size distribution of porous media MP1 and MP2

Both media show a narrow distribution, with the dominant pore sizes being 0.02 μm and 0.05 μm for MP1 and MP2 respectively.

2.7 Ink characterization

The ink properties, which were measured, were surface tension, viscosity, and filtercake resistance. The surface tension was measured by the tensiometer with a De-Nuoy ring, while the viscosity was measured with a Bohlin rheometer using a concentric double-gap cylindrical geometry. The filtercake resistance, which is not a routinely measured quantity, applies to the "cake" of pigments,

which is formed above the inkjet coating, when the vehicle of the pigmented ink is absorbed. The theory of filtercake resistance is described in the section 2.8.2.

2.7.1 Ink specifications

Two types of inks were primarily used- pigmented, and dye based. The following notation will be used to specify the various inks.

1) IP1 (pigmented, black)
2) IP2 (pigmented, black)
3) IP3 (pigmented, yellow)
4) ID1 (dye-based, yellow)
5) ID2 (dye-based, yellow)

The particle size data, obtained from the manufacturer, for the pigmented inks, is shown in Table 2.3. The ink IP3 has a bimodal distribution of pigment sizes.

Table 2.3 Pigmented ink particle size distribution data

Ink	Pigment diameter (nm)	Width of distribution (nm)
IP1	96.9	75.2
IP2	117.7	118.1
IP3	78 26.5	75.2 18.3

The ink surface tensions were measured by the Sigma70 tensiometer using a standard De-Nuoy ring. The results are shown in Table 2.4. The presence of

surfactants in the inks, which are water-based, reduces the surface tension to meet the various requirements of the overall printing process.

Table 2.4 Surface tension data

	IP1	IP2	IP3	ID1	ID2
Mean surface tension (dyne/cm)	53.39	40.00	24.22	33.26	30.43
Std. Dev.	0.46	0.28	0.17	0.14	0.22

The viscosity was measured by a CVO rheometer manufactured by Bohlin Instruments. The results are shown in Table 2.5. The results are within the expected ranges. The pigmented inks can be seen to have slightly higher viscosities.

Table 2.5 Viscosity data

	IP1	IP2	IP3	ID1	ID2
Mean viscosity, (cP)	5.2	5.7	6.3	4.9	2.8
Std. Dev.	1.64	1.25	1.61	2.6	0.27

2.7.2 Filtercake resistance

The theory of filtration was adapted to the pigmented ink absorption process to evaluate the ability of the pigment cake to hinder further absorption of the ink into the coating [31]. The specific filtercake resistance α, as defined in equation 2.4, is an easily determinable quantity to compare the filtercake-forming

ability of pigmented inks. The experimental procedure consists of applying air pressure to force ink through a 0.1micron polycarbonate filter, into a blotter paper, for a fixed amount of time. The instrument used was a gravimetric water retention meter manufactured by Kaltec Scientific. The experimental setup can be seen in the following Figure.

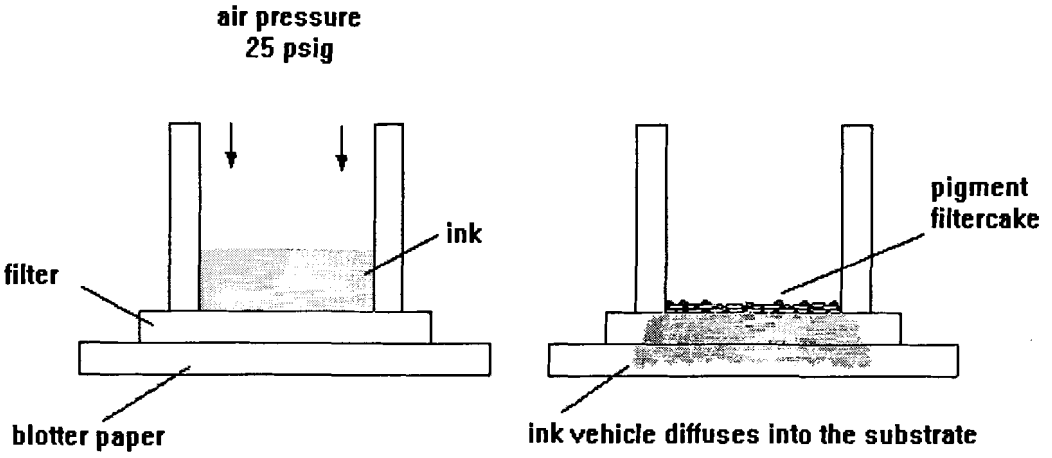

Figure 2.13 Pressurized filtration apparatus

The basic filtration equation is written as

$$\Delta P = \frac{4.17 u \mu (s_p / v_p)^2 (1-\varepsilon) m_c}{\rho_p A (\varepsilon)^3} \tag{2.4}$$

where s_p is the surface area of a single particle, v_p is the volume of a single particle, ρ_p is the particle density and ε is the void fraction of the cake. The specific filtercake resistance α is defined as

$$\alpha = \frac{\Delta p \cdot A}{\mu \cdot u \cdot m_c} \tag{2.5}$$

where Δp is the overall pressure drop = Δp over cake + Δp over filter medium,

A is the filter area measured perpendicular to the direction of the flow, and

μ is the viscosity of the filtrate. The term u in Eq. (2.4) is defined as

$$u = \frac{dV/dt}{A} \tag{2.6}$$

where V is the volume of filtrate collected from the start of the filtration to time t.

The total mass of solid in the cake m_c, is defined as

$m_c = V \cdot c$ where c is the mass of the particles deposited in the filter per unit volume of filtrate.

Another way of estimating the value of α is a graphical method, which uses different values of t for filtration, as opposed to the above method, for which a single measurement can suffice. The graphical method involves the following calculations.

For constant pressure filtration

$$\frac{\mu \cdot R_m}{A \cdot \Delta p} = \left(\frac{dt}{dV}\right)_0 = \frac{1}{q_0} \tag{2.7}$$

where the subscript 0 refers to the value at time =0, and R_m is the filter medium resistance.

The filtration equation can be written as

$$\left(\frac{dt}{dV}\right) = \frac{1}{q} = K_c + \frac{1}{q_0} \tag{2.8}$$

where

$$K_c = \frac{\mu \cdot c \cdot \alpha}{A^2 \cdot \Delta p} \tag{2.9}$$

Integrating Eq.(2.8) between the limits (0,0) and (t,V) gives

$$\frac{t}{V} = \left(\frac{K_c}{2}\right) \cdot V + \frac{1}{q_0} \tag{2.10}$$

A plot of t/V vs. V is linear with a slope equal to $K_c/2$ and an intercept of $1/q_0$

A pressure of 25 psig, and t values of the order of 30 seconds were used for the measurements.

The experimentally measured filtercake resistances for the three pigmented inks are shown in Table 2.6. Filtration was carried out for 30 seconds to determine the calculated value of α, while the graphical method used measurements done at 15, 30, and 60 s. The detailed calculations are available in Appendix A.

Table 2.6 Filtercake resistances of pigmented inks

Ink	IP1		IP2		IP3	
	Calculated value	Graphical method	Calculated value	Graphical method	Calculated Value	Graphical method
Specific filtercake resistance (α), m/kg	1.2×10^{15}	2.0×10^{15}	1.0×10^{15}	1.9×10^{15}	2.1×10^{15}	4.1×10^{15}

The graphical method, which uses a best-fit curve to calculate α, is more reliable of the two methods, and from the above values, IP3 shows a relatively higher value, implying more resistance to flow. These results are consistent with the particle size distributions: fine particles should lead to high resistances.

2.8 Ink-media interaction

The third set of experiments was aimed at studying the interaction between the ink and media. The ink absorption rates and the dynamic gloss of printed ink areas were studied for this purpose. The dynamic gloss results will be discussed in a later chapter.

2.8.1 Bristow absorption

The absorption rates of the inks were measured on all the substrates using the Bristow wheel. The instrument, as shown in Figure 2.14, consists of a wheel, which can rotate at a fixed speed. A rectangular strip of the media is attached to the rotating wheel, and a known amount of ink is applied to the media through the ink trough, which holds the ink by surface tension. The rate of absorption can be calculated from the area of the ink trace, the speed of the wheel, and the amount of the ink used [32].

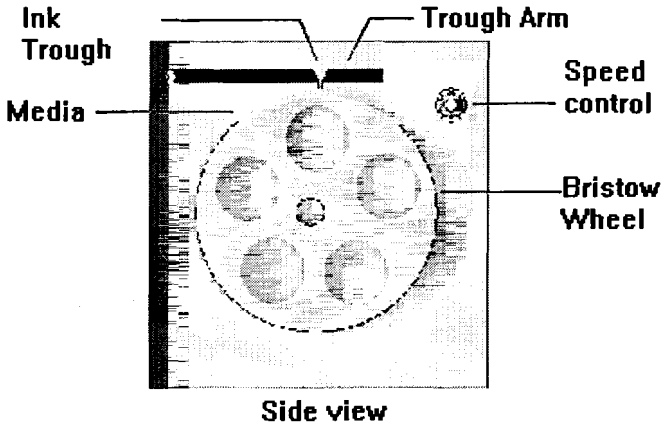

Figure 2.14 The Bristow wheel instrument

A typical Bristow wheel curve shown in Figure 2.15, can be expressed as

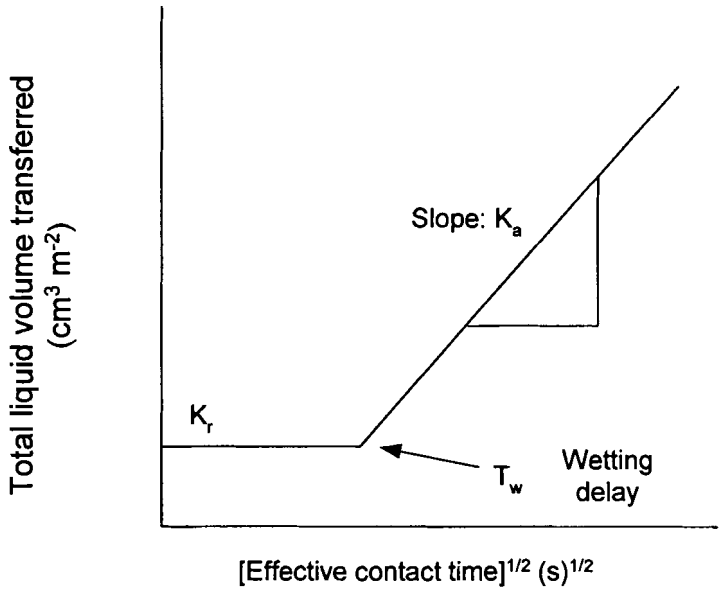

Figure 2.15 Typical Bristow wheel curves

$$V=K_a t^{1/2} + K_r \qquad (2.11)$$

Where V is the volume of ink transferred to the paper (cm^3m^{-2})

K_a is called the Bristow absorption coefficient ($cm^3m^{-2}s^{-0.5}$), and K_r is the roughness coefficient (cm^3m^{-2}), and t is the effective contact time, measured in seconds. The typical curves for paper coatings show an initial horizontal portion, which corresponds to a wetting delay, during which the surface pores are filled. The slope of the inclined part of the curve serves to characterize the ink flux, although with slightly different units. The y-intercept K_r, characterizes the surface roughness.

For the experiment, the amount of ink used had to be adjusted in order to obtain the entire trace on the given fixed length of the media strip, which had to be continuous. The same amount of ink was used for all experiments (10 μL), after observing an upward shift in curves measured with higher amounts of ink, for the same conditions of speed. The areas of the ink traces were measured by image processing software due to the non-rectangular shapes of the traces obtained.

The Bristow wheel tests were conducted for a total of 30 combinations, with the five inks and six media. The resulting curves are shown in the proceeding section. Each combination was repeated 4 times.

2.8.2 Bristow absorption results

The data is presented graphically for each medium with a particular ink, and also a numerical comparison of the values of K_r for different combinations in Figs.2.16-2.19. Some combinations of ink and media caused the media to scrape off during the test and are not reported.

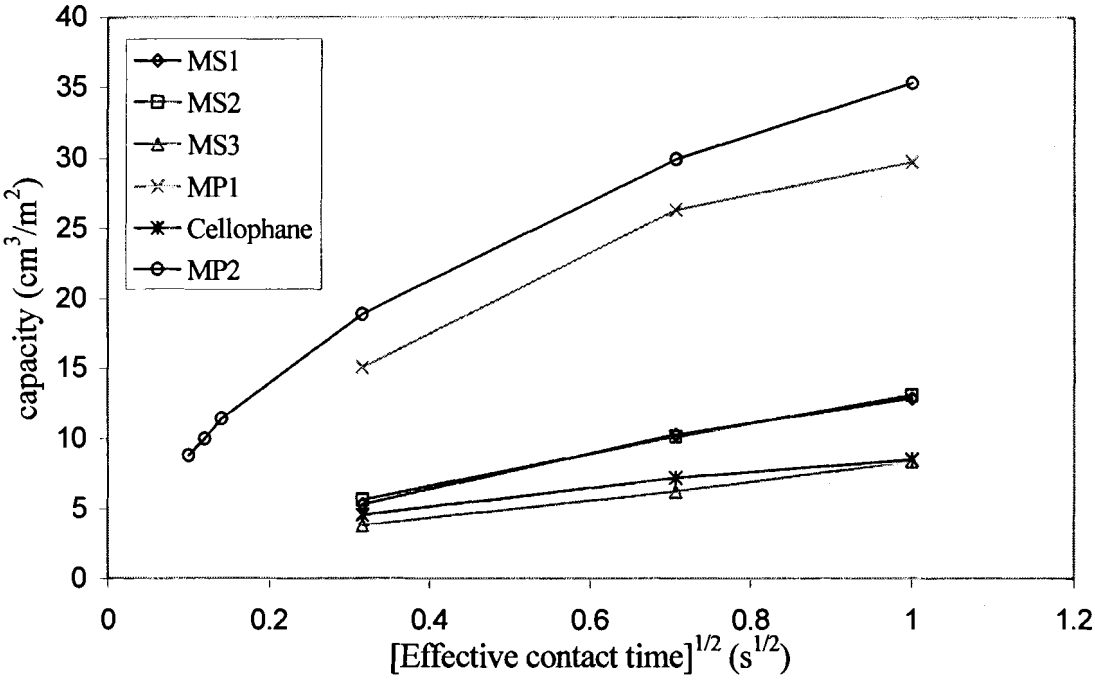

Figure 2.16 Bristow absorption curves for ink IP1 with different media

The porous media show much higher absorption rates than the swellable media, which is understandable in view of the rapid uptake capacity of the porous coatings. Medium MP2 has a higher absorption rate than MP1, which could be explained by the higher total porous volume and a higher average pore diameter, as seen from the mercury porosimetry results.

However the comparison of short-time absorption fluxes with saturation-level fluxes may be erroneous to help understand the behavior of porous and swellable media. The swellable media were observed to swell and absorb liquid at a lower rate than the porous media, which may explain the general trend of low Bristow absorption coefficients of the swellable media.

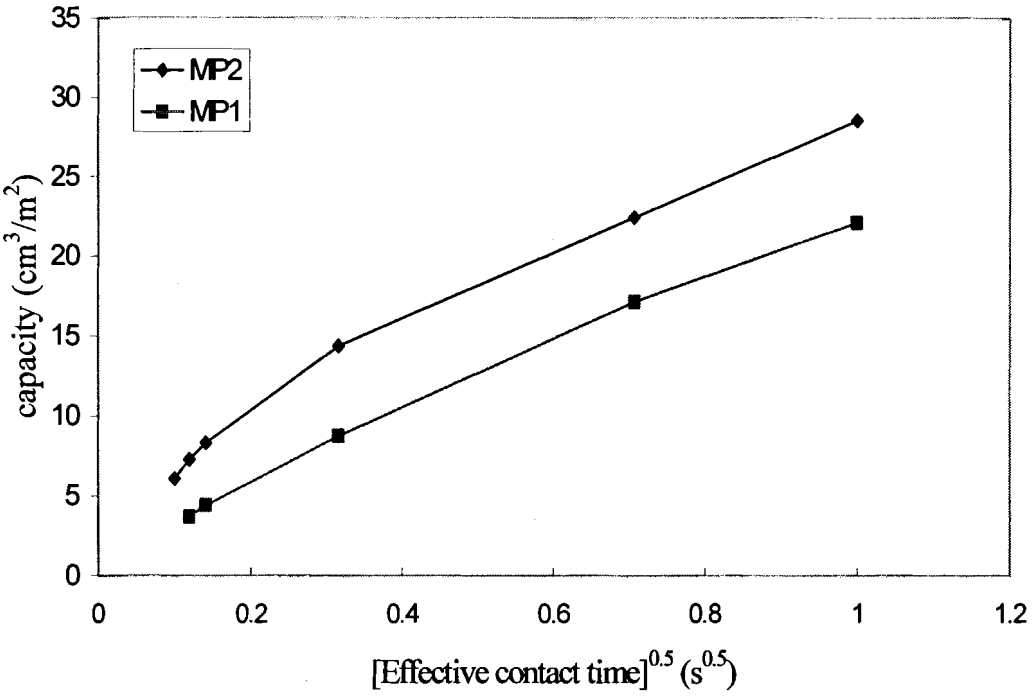

Figure 2.17 Bristow absorption curves for ink IP2 with different media

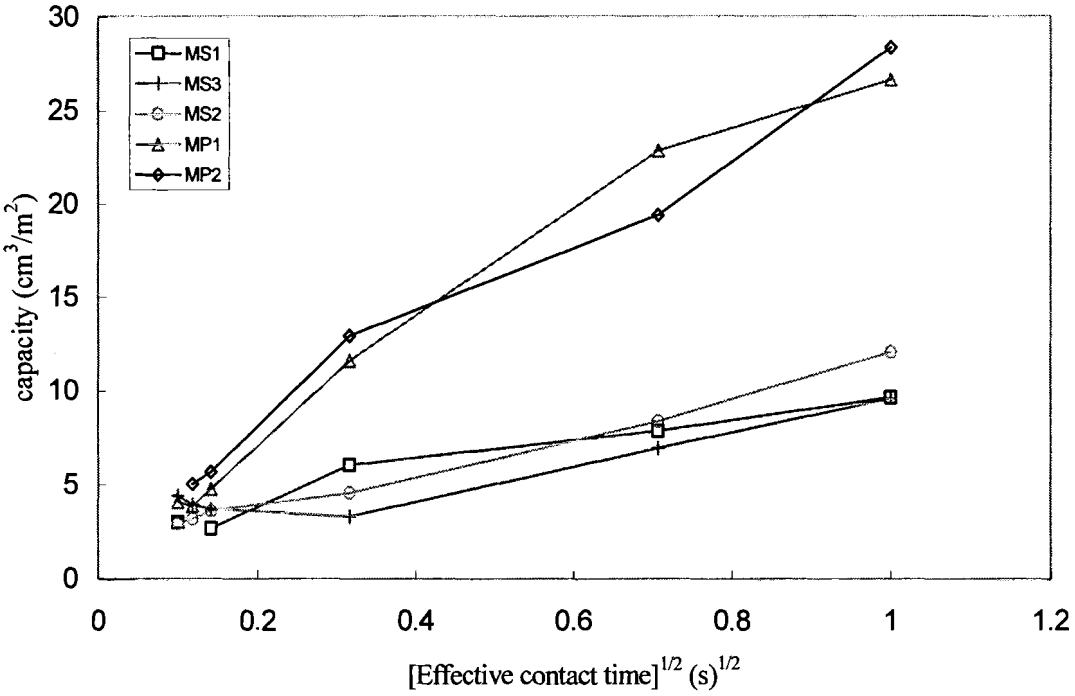

Figure 2.18 Bristow absorption curves for ink IP3 with different media

The results with ink IP3 show a similar trend, and another observation is that the media MP2 shows a consistently higher absorption rate with both pigmented inks shown above.

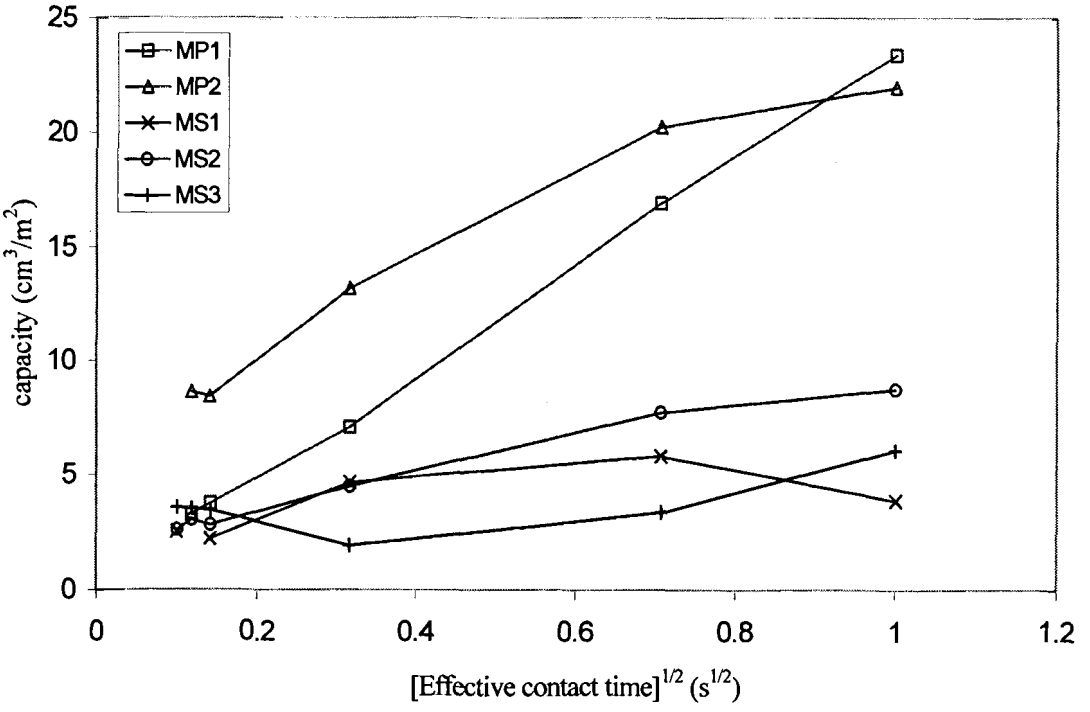

Figure 2.19 Bristow absorption curves for ink ID1 with different media

Figure 2.19 shows similar results for the dye-based ink ID1; however, the difference between the two porous media is more pronounced than in the earlier cases. The complete results are shown in the form of Bristow absorption coefficients for all the different ink and media combinations.

Table 2.7 Bristow absorption coefficients

Ink	K_a ($cm^3 m^{-2} s^{-0.5}$)						
	MP1	MP2	MS1	MS2	MS3	MS4	Cello-phane
IP1	21.85	24.22	11.10	10.91	6.61	16.7	5.79
IP2	21.01	24.43				8.3	
IP3	22.34	22.28	5.23	10.94	9.19	13.9	
ID1	23.29	15.83	2.93	7.07	5.90	13.7	
ID2	21.72	23.20				22.5	

As seen in Table 2.7, the swellable media have lower absorption rates than the porous media, and the porous media seem to be indifferent to the effects of ink type; porous or dye. However, media MS4 shows the highest absorption rates among the swellable media, with values comparable to the porous media, with ID2. The partially vacant columns for the swellable media are due to the problems caused by the swelling of the coating when the ink is deposited. This causes the metal ink dispenser to scrape some of the wet coating-ink mixture off the substrate, rendering the measurement invalid. The values of the roughness coefficient K_r are not presented here, due to the lack of confidence in measuring the high-speed data points around 10 cm/s, which were close to the operating limit of the instrument, and an artificially high amount of ink deposition is suspected due to loss of contact between the ink trough and the substrate, due to the high speed of the wheel.

An attempt was made to overcome the problem of scraping, by artificially lifting the trough a few microns above the substrate using a rod, which supported the weight of the trough. The rod was placed on a platform whose vertical

displacement could be controlled by turning a knob. The scraping was effectively eliminated; however controlling the gap between the trough bottom and the substrate precisely presented another difficulty. A micrometer screw was added in series to the rod assembly to quantitatively know the gap for each measurement, but precise control and reproducibility were difficult to achieve. The Bristow absorption results of a few ink-media combinations are therefore not reported.

2.9 Summarized ink and media properties

Tables 2.8 and 2.9 present a summary of the media and ink properties studied.

Table 2.8 A summary of media properties

Media	AFM Ra (μm)	Stylus Ra (μm)	Static Contact angle of water (degrees)	Receding Contact angle of water (degrees)	Advancing Contact angle of water (degrees)	Silicone oil absorp-tion (g/m^2)	Water absorp-tion (g/m^2)	Mean pore Size (μm)
MP1	0.06	2.35	50.1	19.9	27.4	10.2	20.41	0.0151
MP2	0.13	1.89	46.6	33.6	76.4	4.04	30.56	0.0214
MS1	0.10	1.56	20.1	40.5	104.4	0.32	16.04	
MS2	0.09	2.66	44.6	0	105.4	4.24	306.6	
MS3	0.23	0.62	58.2	34.4	108.2	2.08	63.78	
MS4		4.16	60.7	26.4	105.8	4.89	27.72	0.095

Table 2.9 A summary of ink properties

Ink	Surface tension (dyne/cm)	Viscosity (cp)	Filtercake Resistance (m/kg)	Percent solids content
ID1	33.26	4.91		
ID2	30.43	2.84		
IP1	53.39	5.21	2.0×10^{15}	9.13
IP2	40.00	5.77	1.9×10^{15}	20.45
IP3	24.22	6.34	4.1×10^{15}	15.68

Chapter 3: Dynamics of Ink Film Leveling

3.1 Problem definition

The leveling dynamics of an ink film during absorption into a substrate determine the final optical print properties. The problem was extensively studied by Desjumaux and Bousfield using a model incorporating the effects of various physical properties of the substrate and ink on the rate of absorption, and the final profile of the ink film [33]. The model was adapted to study the coalescence and leveling of two adjacent ink drops, a situation which is encountered during inkjet printing. The model was also used to predict the development of the gloss of the ink layer during its imbibition by the media. This chapter describes the model and the predicted results for the film profile assuming a spherical initial geometry. The subject of the predicted gloss development and the comparison with the experimental results will be discussed in the next chapter.

3.2 Model description

Two hemispherical drops in contact immediately after deposition was the assumed time scale and geometry for the problem of interest. The event of leveling is preceded by the formation of a highly viscous layer called filtercake above the coating surface. This layer is composed of ink pigments and binders, which are deposited on the coating surface, while some of the ink phase is absorbed into the substrate by capillary effects and diffusion [34]. The rate of diffusion of the

pigments from the filtercake into the bulk is assumed to be much smaller as compared to the time scale of leveling which is of the order of milliseconds.

The momentum equations are solved along with the mass balance equations for the penetration of ink into the substrate and the Laplace-Young equation relating the pressure to the surface tension. The profile of the ink film is modeled as a function of time, and is obtained by solving a fourth order partial differential equation relating the ink film height to position and time. The effect of disjoining pressure was neglected in this study. The following Figure illustrates the geometry of the initial identically similar ink drops.

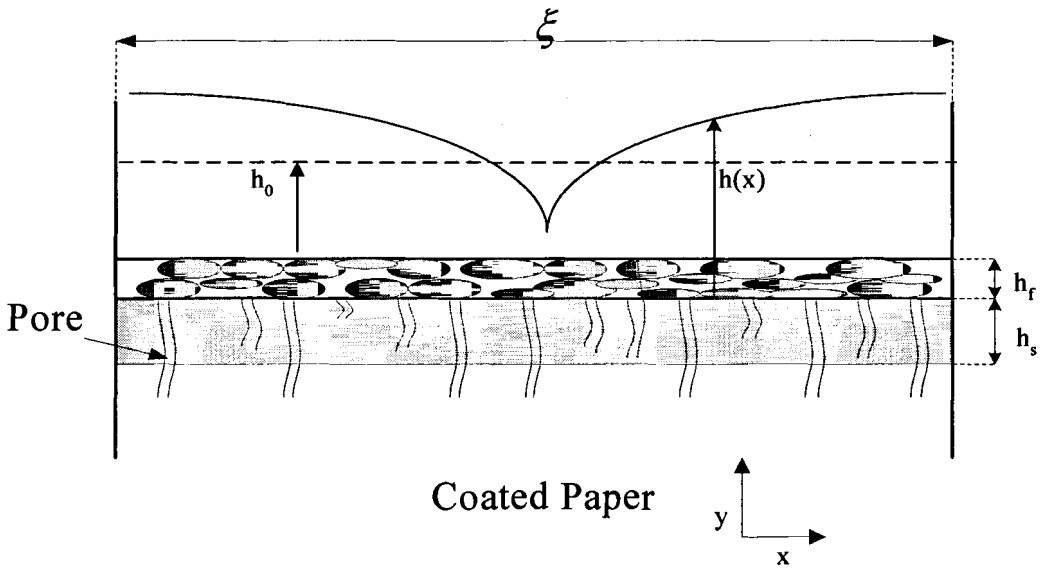

Figure 3.1 Cross-section of a fluid layer on a porous surface.

In the Figure 3.1, h_o is the thickness if leveling is complete, ξ, the wavelength of disturbance, h(x), the distance to the free surface from substrate, h_f, the filtercake thickness and h_s, the depth of penetration.

3.2.1 Equations of motion

If the film thickness, h_0, is very small compared to ξ, the wavelength of disturbance, and for low values of the Reynolds number, lubrication type arguments are valid to reduce the two-dimensional transient problem to a one-dimensional transient problem. For the film thickness and viscosity, μ, involved in printing, gravity is assumed to have no effect. The x and y momentum terms of Navier-Stokes equations for thin films are given as

$$\frac{\partial P}{\partial x} = \mu \cdot \frac{\partial^2 v_x}{\partial y^2} \tag{3.1}$$

$$\frac{\partial P}{\partial y} = 0 \tag{3.2}$$

where P is the local pressure, μ, the viscosity of the fluid, v_x, the velocity of fluid parallel to the substrate surface and y, the direction perpendicular to the substrate surface. Equation (3.2) shows that P is not a function of the y-coordinate. The x-momentum equation can be integrated with both no-slip condition at the top of the filtercake and no-shear condition at the free surface as

$$v_x = 0 \quad @ \quad y = h_f \tag{3.3}$$

$$\frac{\partial v_x}{\partial y} = 0 \; @ \quad y = h \tag{3.4}$$

Starting with the Laplace equation, the pressure jump across the free surface in the limit of thin films is given as

$$P = -\gamma \cdot \frac{\partial^2 h}{\partial x^2} \tag{3.5}$$

where γ is the surface tension. Using a mass-shell balance on a slice, a relationship between the penetration velocity, v, normal to the substrate, the velocity in the x-direction and the free surface motion is established as follows.

$$\frac{\partial h}{\partial t} = -\frac{\partial}{\partial x}\left[\int_{h_f}^{h} v_x . dy\right] - v \tag{3.6}$$

where v is the velocity normal to the substrate due to absorption and diffusion. Note that if there is no leveling, the free surface decreases as v. It is possible to obtain the same result with using the Leibnitz rule and the kinematic condition on the integrated continuity equation.

By integrating eq. (3.1) and using the two boundary conditions given in Eq. (3.3) and (3.4), an expression of the velocity profile is obtained as

$$v_x = \left(\frac{1}{2.\mu} \cdot \frac{\partial P}{\partial x}\right) \cdot \left(y^2 - h_f^2\right) - \left(\frac{1}{\mu} \cdot \frac{\partial P}{\partial x} \cdot h\right) \cdot \left(y - h_f\right) \tag{3.7}$$

By substituting the derivative of the pressure in Eq. (3.5) into Eq. (3.7), an expression of the velocity profile is obtained in terms of curvature of the surface as

$$v_x = -\frac{\gamma}{3\cdot\mu}\cdot\frac{\partial^3 h}{\partial x^3}\cdot\left(y^2 - h_f^2\right) + \frac{\gamma}{\mu}\cdot\frac{\partial^3 h}{\partial x^3}\cdot h\cdot\left(y - h_f\right) \tag{3.8}$$

By inserting the velocity profile into the mass balance relation, the final equation is obtained as

$$\frac{\partial h}{\partial t} = -v - \frac{\gamma}{3\cdot\mu}\cdot\frac{\partial}{\partial x}\cdot\left(\frac{\partial^3 h}{\partial x^3}\cdot\left(h - h_f\right)^3\right) \tag{3.9}$$

In addition of this working equation, two other mass balances link the penetration depth with the growth of the filtercake as

$$\frac{\partial h_s}{\partial t} = v\cdot\frac{1}{\varepsilon} \tag{3.10}$$

$$\frac{\partial h_f}{\partial t} = v\cdot\frac{\phi}{\phi_m} \tag{3.11}$$

where ε is the void fraction of the substrate, ϕ, the volume fraction of solids in the ink and ϕ_m, the maximum flowing volume fraction of the ink. The net result is a set of equations that link the surface-tension-driven leveling of the fluid layer with the removal of ink mobile phase from the ink film layer.

To solve the set of equations, four boundary conditions are necessary. The ink film surface is taken to be symmetrical. This sets the first and third derivatives to be zero at the boundaries as

$$\left(\frac{\partial h}{\partial x}\right)\Bigg|_{x=0} = 0 \tag{3.12}$$

$$\left(\frac{\partial h}{\partial x}\right)\Bigg|_{x=\xi} = 0 \tag{3.13}$$

$$\left(\frac{\partial^3 h}{\partial x^3}\right)\Bigg|_{x=0} = 0 \tag{3.14}$$

$$\left(\frac{\partial^3 h}{\partial x^3}\right)\Bigg|_{x=\xi} = 0 \tag{3.15}$$

If a solution is sought as

$$h(x,t) = h_0 + \varepsilon_0 \cdot \cos\left(\frac{2\pi \cdot x}{\xi}\right) \cdot e^{-\beta \cdot t} \tag{3.16}$$

where ε_0 is a small disturbance amplitude, h, the ink film shape function of x, the direction parallel to the substrate surface, and t, the time, h_0, the initial ink film thickness and ξ, the wavelength of disturbance. Through linear analysis the exponential factor β is a constant given as

$$\beta = \frac{16}{3} \cdot \gamma \cdot \pi^4 \cdot \frac{h_0^3}{\mu \cdot \xi^4} \tag{3.17}$$

where γ is the surface tension of the fluid and μ, the viscosity of the fluid. The leveling rate is of an exponential form with the rate constant, proportional to the viscosity and the surface tension, depending on the third power of film thickness and the fourth power of the wavelength.

The equations that describe the removal of the ink mobile phase into the coated paper are developed further. The penetration may be a combination of capillary absorption in the pores of the substrate and diffusion by swelling of the latex matrix. Namely, the velocity of penetration is function of two different terms,

v_c and v_d, representing respectively the velocity of penetration by capillary pressure effects and by diffusive effects. The total velocity of penetration is taken as

$$v = v_c \cdot \varepsilon + v_d \cdot (1-\varepsilon) \cdot (1-PVC) \tag{3.18}$$

where ε is the void fraction and PVC, the pigment volume concentration.

The laminar flow in a porous media is given by Darcy's law. For flow in the substrate, the expression is

$$v_{c_s} = \frac{K_s . \Delta P_s}{\mu' . h_s} \tag{3.19}$$

where K_s is the Darcy's law constant of the substrate, μ', the viscosity of the mobile phase and ΔP_s, the pressure drop across the substrate front in a cylindrical pore. In the same way, the laminar flow through the filtercake is given as

$$v_{c_f} = \frac{K_f \cdot \Delta P_f}{\mu' \cdot h_f} \tag{3.20}$$

where K_f is the Darcy coefficient of the filtercake and ΔP_f, the pressure drop across the filtercake front. The total pressure drop between the fluid layer and the curved interfaces is assumed to be the standard expression for a fluid in a cylindrical pore.

$$\Delta P = \Delta P_f + \Delta P_s = 2\gamma \cos(\theta) / R_p \tag{3.21}$$

where θ is the contact angle and R_p, the pore radius.

Combining eq. (3.19), (3.20) and (3.21) gives

$$v_c = \frac{2\gamma \cdot \cos(\theta)/R_p}{\mu' \cdot \left[\frac{h_f}{K_f} + \frac{h_s}{K_s}\right]} \tag{3.22}$$

The dynamic contact angle is assumed not to be a function of the rate of capillary rise.

This expression should be valid for the flow through different porous media with pressure drop of Eq. (3.21). In the model, the filtercake thickness and depth of penetration increases with time as shown in Eqs. (3.11) and (3.10).

A factor which is not addressed by the capillary sorption approach is the ability of many ink solvents to absorb into or swell polymer films. To describe this diffusive mechanism, the equation for the diffusion of a component A through a semi-infinite slab of component B (Bird *et al.*, 1960) [35] is simplified to obtain the penetration velocity by diffusive effects as

$$v_d = \sqrt{\frac{D_{AB}}{\pi \cdot t}} \tag{3.23}$$

where D_{AB} is the diffusion coefficient and t is time.

The model describes the film profile "h" as a function of time by Eqs. (3.9), (3.11), (3.18), (3.22) and (3.23). Finite difference techniques are used to calculate the derivative in Eq.(3.9). Euler time integration is used to calculate the change in the profile, the filtercake thickness and depth of penetration.

3.2.2 Results

The actual profile of the film which is formed after the merging of the two adjacent ink drops was plotted as a function of time and can be seen in Figure 3.2. The time scale of leveling of such an initial geometry is of the order of milliseconds. The effects of various parameters on the leveling time were also investigated. The parameters which are primarily found to affect the time of

leveling are viscosity, surface tension, and the wavelength of disturbance. As expected from the postulated solution, the leveling time, which can be looked upon as the time taken by the film to attain a final smooth profile, increases with the disturbance wavelength.

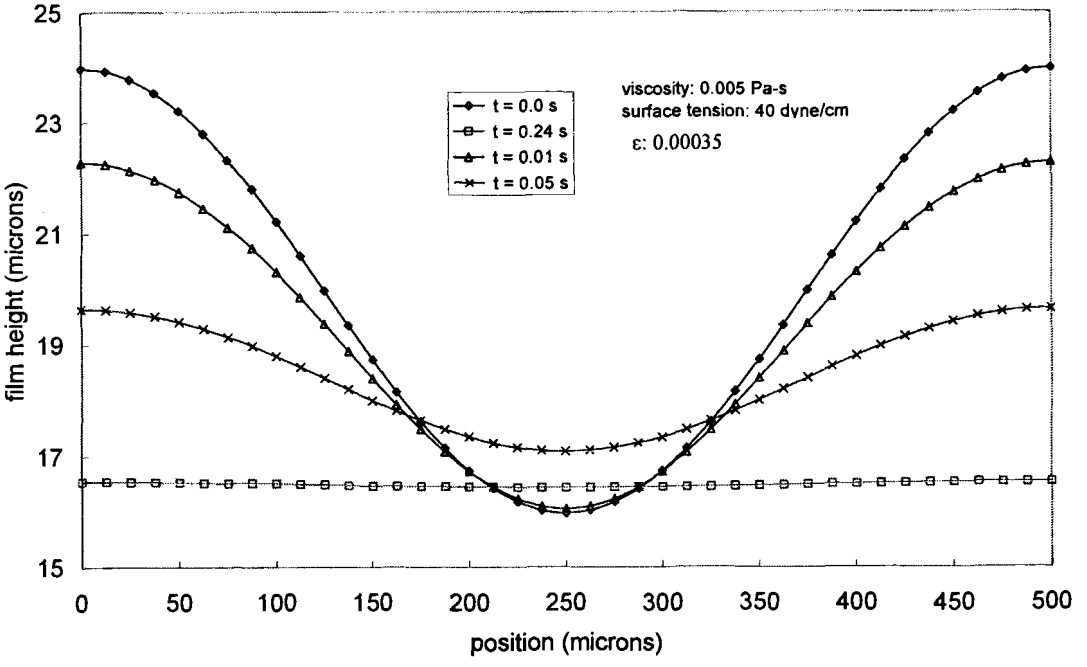

Figure 3.2 Ink film height as a function of time on a coated substrate

Lowering viscosity is found to reduce leveling time. The effect of two values of viscosity while holding the other parameters constant, can be seen in Figure 3.3.

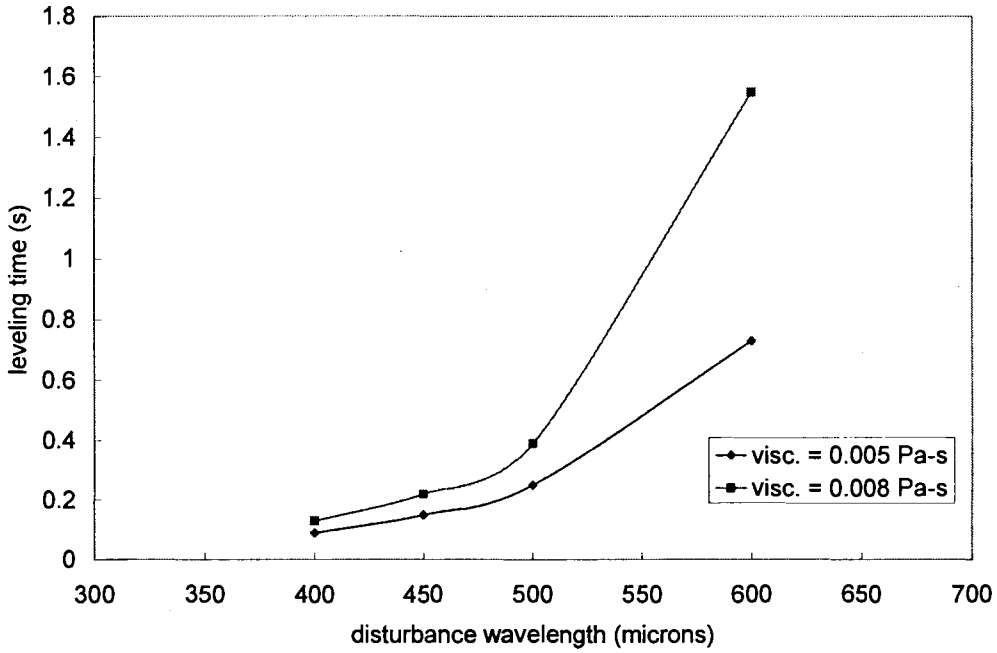

Figure 3.3 Effect of viscosity on leveling time for viscosities of 0.005 and 0.008 Pa-s

The film profiles predicted by the model for two different viscosity values at the same instant of time are depicted in Figure 3.4.

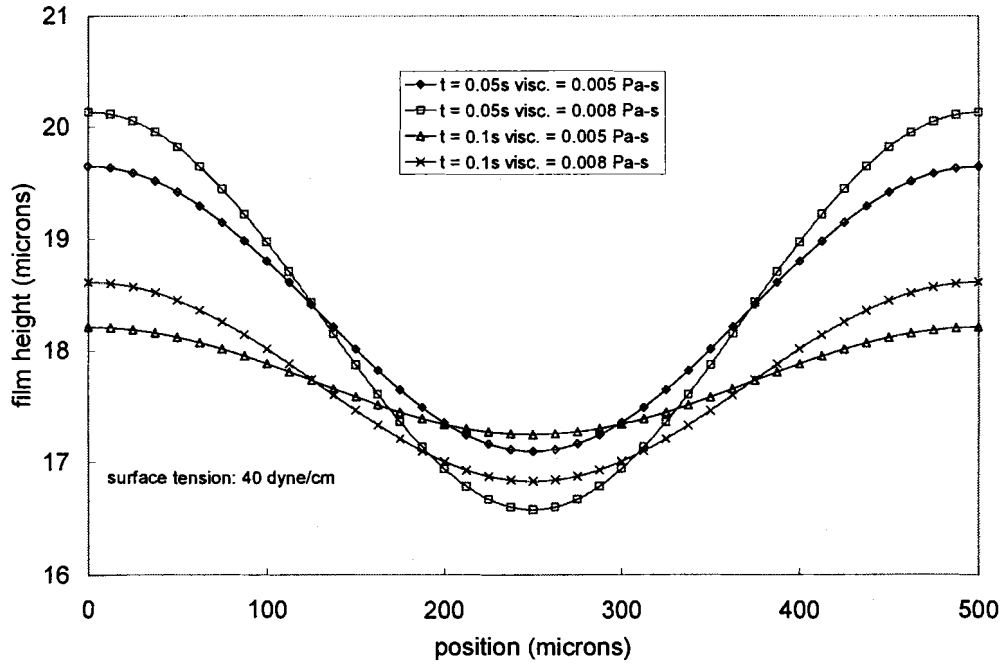

Figure 3.4 Effect of viscosity on ink film profiles

The ink with the lower viscosity can be seen to level at a higher rate and the two profiles at any given instant of time are found to be similar.

In the reverse fashion, increasing the surface tension reduces the time of leveling. The effects of two different values of surface tension are depicted in Figure 3.5. The film profiles predicted by the model for two different values of surface tension at the same instant of time are depicted in Figure 3.6.

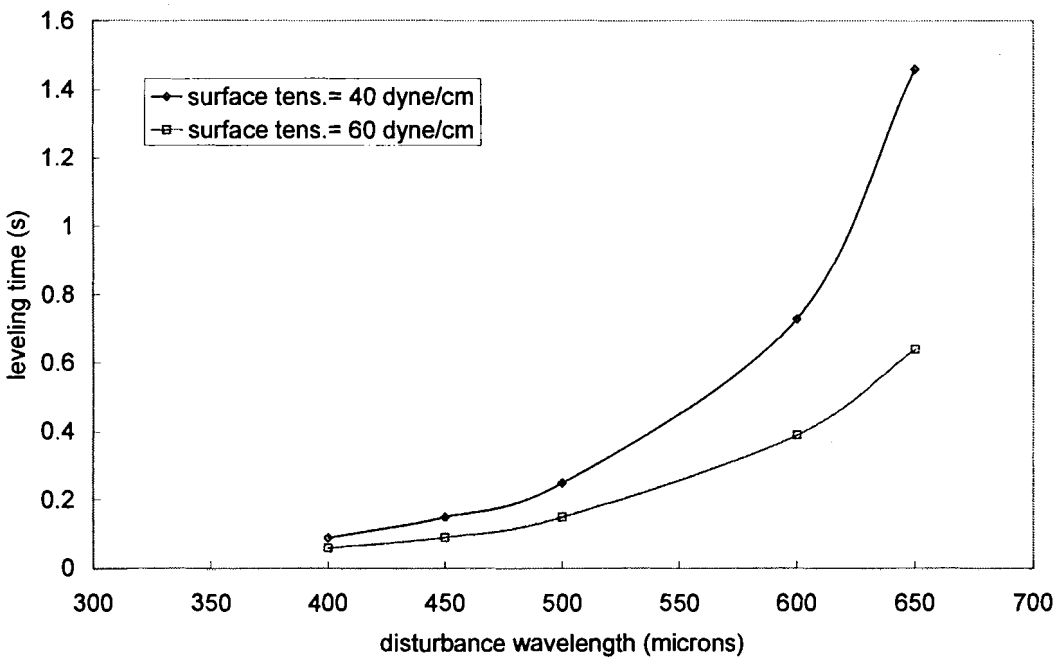

Figure 3.5 Effect of surface tension on leveling time for surface tension of 40 and 60 N/m

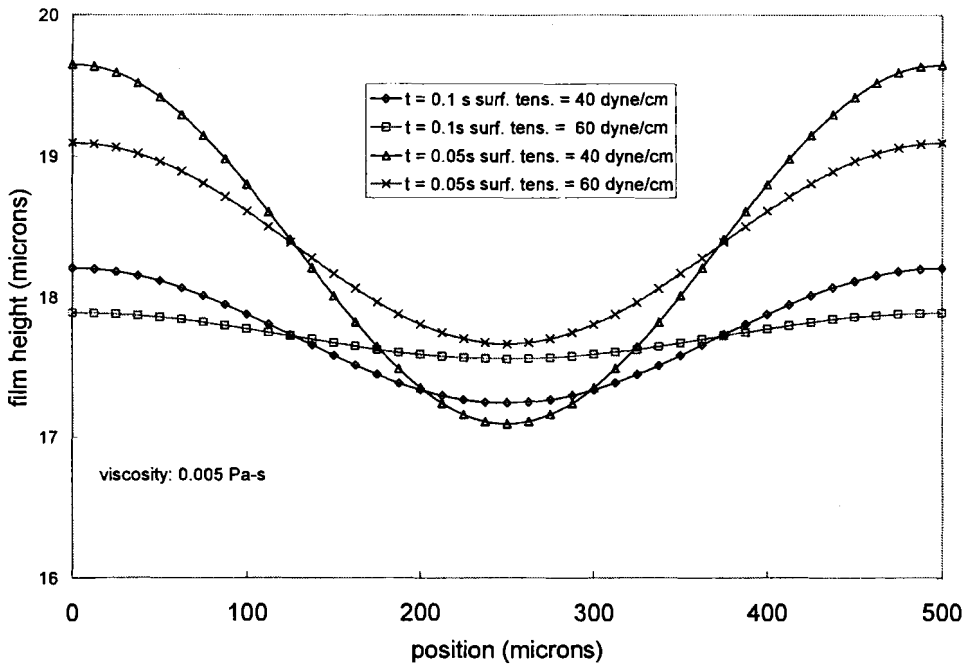

Figure 3.6 Effect of surface tension on ink film profiles

The distinct nature of the two profiles at any instant of time is evident from the above Figure. The rate constant of leveling β, in the linear analysis of Eq. (3.16) predicts the effects of viscosity, surface tension, and the disturbance wavelength. The above results are seen to be in agreement with those predicted from the linear analysis. The leveling time is found to decrease with a lowering of the Darcy law constant for the filtercake ,K_f , only by large changes (factor of $10^{\pm 2}$), while the constant for the substrate, K_s, does not affect the leveling even by large changes of a factor of 10^{+4}.

The model was modified to account for the swelling effects of polymeric coatings, and the roughness of the coatings during wetting, which are important

factors controlling the gloss development. The results of the gloss studies and the related model modifications will be discussed in the next chapter.

Chapter 4: Dynamic Gloss Results

The final part of the study focused on the measurement of the gloss during the initial few seconds, when the effects of most of the controlling factors are most dominant. In order to capture the dynamics at very short time scales, a setup by which the gloss could be continuously monitored with a high data acquisition frequency was used, with a one-millisecond resolution. This chapter describes the experimental apparatus, the experimental gloss results, and the gloss predicted by the model.

4.1 Factors affecting gloss development

The model described in the previous chapter was adapted to predict the value of gloss as the ink layer is absorbed into the coating. Some of the assumptions made in the model are that the gloss of the print is affected by the ink pigment size, the refractive index of the ink, the smoothness of the ink layer, and the swellability of the base. The roughness of the wet polymeric coating were found to play an important role in the gloss development process of the swellable coatings. The ink gloss with the non-swellable media is affected by the gloss of the media without ink. The "wet roughness" of the media used in the calculations was an empirical correlation to the values measured by the stylus profilometer using water as the wetting agent. The values of the wet roughness as measured, and as fed to the model are shown in Table 4.1

Table 4.1 Wet media roughness values

Media	Stylus roughness wet (microns)	Model roughness
MS1	2.45	162 nm
MP1	1.33	156 nm
MS2	9.12	197 nm
MS3	5.1	184 nm
MS4	5.4	188 nm
MP2	2.5	170 nm

The gloss is expected to drop when the planar film surface is broken by the pigments, as seen in Fig. 4.1. The relatively non-uniform pigment layer causes a drop in overall gloss. The factors controlling the gloss were decided in the model using the following criteria. The pigment size was taken as the sole contributor to the gloss unless if the media gloss was lower, in which case the media roughness and the pigment size were taken to contribute equally. For cases of low solid volume fraction of inks, or dye based inks, the media roughness was used as the primary contributor. For high swelling media, the wet roughness was used for the gloss calculation, while a function of the ratio of the ink film height above the pigment layer to the initial height of the ink layer was used for the low swelling media. The equations and the calculation scheme are described below, and in Fig. 4.2. The model calculations were performed till the ink film layer was 1 nm thick.

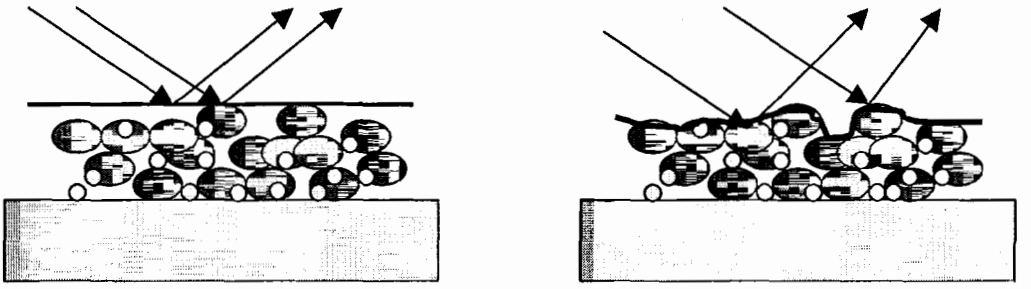

Figure 4.1 Gloss reduction during the absorption of pigmented ink film

The equation used to calculate the gloss was adapted from the equations of Lee and Chinmayanandam, described in Chapter 3. The basic form of the equation is given below

$$\frac{I}{I_o} = f(n,i)\exp[-(4\pi\sigma\cos i/\lambda)^2] \qquad (4.1)$$

where I and I_o are the specularly reflected and incident light intensities, respectively, f(n,i) is the Fresnel coefficient of specular reflection as a function of refractive index n and angle of incident light i, σ the standard deviation of the surface roughness, and λ is the wavelength of incident light. Figure 4.2 shows the scheme followed in the gloss calculations.

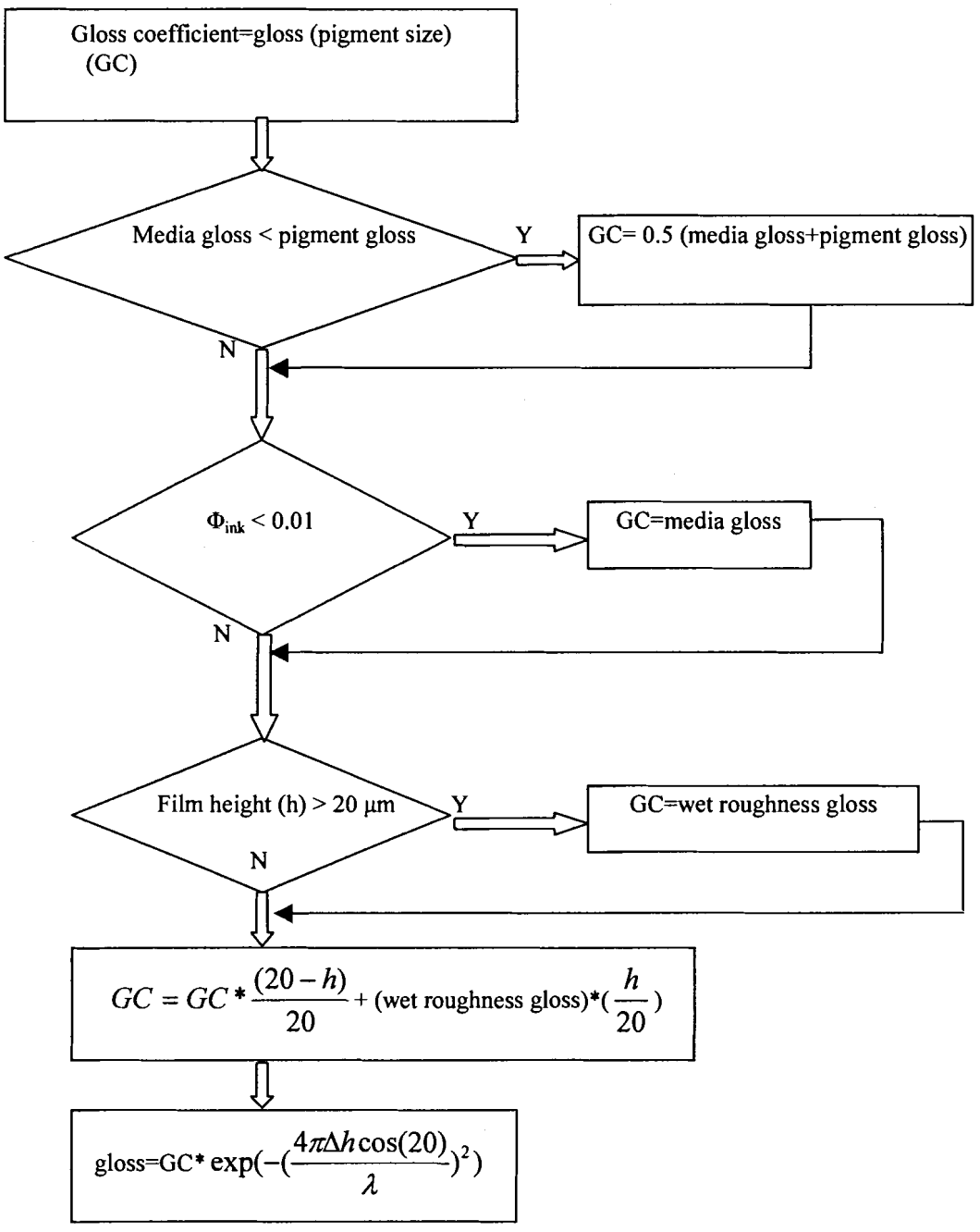

where Δh is the height difference of the end points of the surface profile

Figure 4.2 Gloss calculation scheme

4.2 Apparatus

The setup used for the experiments consisted of an inkjet printer (970 Cxi inkjet, Hewlett-Packard) connected to a computer as depicted in Figure 4.3. A Visual Basic program was used to control the data acquisition using modified PCL files to control the printhead motion and ink deposition. The program enabled the capture of 30,000 data points at a frequency of $1ms^{-1}$. The printhead was controlled so as to fire all the nozzles and print a rectangular block approximately 10 mm x 90 mm. The gloss was measured by reflecting a 680 nm, 5 mW laser beam off the printed block and collecting the reflected light with a detector, which was also connected to the computer. The printer had to disassembled to make the print area accessible to the laser arrangement. The printer cover had to be removed, and a hole had to be drilled in the top metal plate to achieve the 20-degree geometry. The plane of the beam was chosen as being perpendicular to the printhead motion to reduce the extraneous data points obtained by the reflection of ambient light from the side of the printhead in a parallel-plane arrangement. The initial data points in the parallel-plane arrangement made it difficult to choose the first data point of interest. The ambient light had an effect of boosting the detector signal, and therefore the experiments were carried out in a dark-room.

An 8 channel 12-bit Analog-Digital board (CIO-DAS08) with a sampling frequency of 20 KHz was used for the data acquisition. The gloss signal was obtained as a voltage signal measured by an analog voltmeter with a range of 0 to 10 volts.

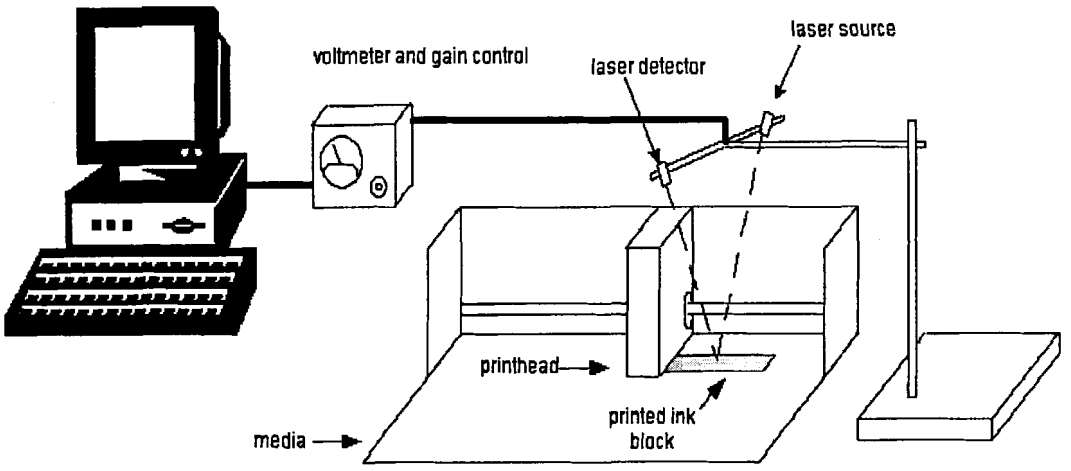

Figure 4.3 Schematic of experimental setup for gloss measurement

4.3 Results

This section describes the comparison of the experimental gloss and the calculated gloss, which is studied as a function of time. The experimental gloss results were calibrated with the values obtained by measuring the gloss of the samples immediately after printing, with a 20° gloss tester (Micro-Tri-Gloss, BYK-Gardner, Germany). The immediate post-printing gloss was used for calibration due to the observation that the gloss of the swellable media kept changing for at least 24 hours. Also, since the inks used were of different colors, individual calibration had to be done, due to the dependence of gloss on the refractive index.

The gloss of dry media and the gloss immediately after printing, was measured by the Micro-Tri-Gloss device, and the results are shown in Table 4.2. The gloss measured immediately after printing is reported as the wet gloss. Due to practical considerations the wet gloss could be measured not before 30 seconds

after printing. The table also includes the values measured 24 hours after printing, and they are reported as the dry gloss values.

Table 4.2 Dry and wet gloss results

	MP1	MP2	MS1	MS2	MS3	MS4
Unprinted	18.3 ± 0.2	10.9 ± 0.4	78.3 ± 0.2	52.5 ± 2.8	62.8 ± 1.0	47.2 ± 0.8
Ink						
IP1 (wet)	79.1	47.3	62.8	25.2	44.4	34.6
IP1 (dry)	68.8	40.5	71.6	47.7	61.7	60.1
IP2 (wet)	20.0	11.7	32.0	26.6	51.5	33.7
IP2 (dry)	10.8	7.2	37.0	16.1	23.8	10.5
IP3 (wet)	65.4	47.3	38.6	15.2	12.4	29.0
IP3 (dry)	72.1	51.8	70.6	28.4	16.0	35.6
ID1 (wet)	18.1	16.0	20.1	5.9	8.8	7.1
ID1 (dry)	17.0	14.1	47.8	24.4	25.1	25.4
ID2 (wet)	18.9	14.7	56.2	32.7	38.5	35.6
ID2 (dry)	17.5	13.0	54.1	32.5	60.3	43.7

The following plots show the experimental values of the different ink-media combinations. Each curve represents the average of five curves. The standard deviation for each curve in Table 4.3 is a percentage of the mean value.

As seen in Figures 4.4 and 4.5, the data of interest begin at approximately 7 to 8 ms after the first point. The porous media show a rapid rise to a final gloss, which occurs within the first 10 ms. The swellable media show an initial rise to a quite sharp peak followed by a slow decay to a final value. The rise may be explained by the leveling of a smooth liquid layer above the coating. The absorption of this ink layer up to the point where the pigments start breaking the liquid surface, takes place in a uniform fashion, helped by the strong surface tension of IP1. The decay in gloss starts when the media swells and adds to the unevenness of the surface profile, covered with the pigment layer. IP1 has a low

solids content, but a high pigment size, hence the wet-roughness and not the pigment size is expected to play a major part in the gloss development within the 20 second period. Table 4.2 shows the gloss after 24 hours, and the porous media show a dry gloss value lower than the wet gloss, implying the effect of high pigment size, which lowers the final gloss after 24 hours. However, the unprinted media gloss is significantly lower than the printed values, suggesting a strong dependence on pigment gloss. The swellable media show an increase in gloss after 24 hours, and a general tendency of the media to recover to the unprinted gloss value is seen. The wet roughness and consequently the wet gloss is observed to be quite lower than the unprinted gloss at approximately 30 seconds, suggesting the ability of IP1 to roughen the swellable media.

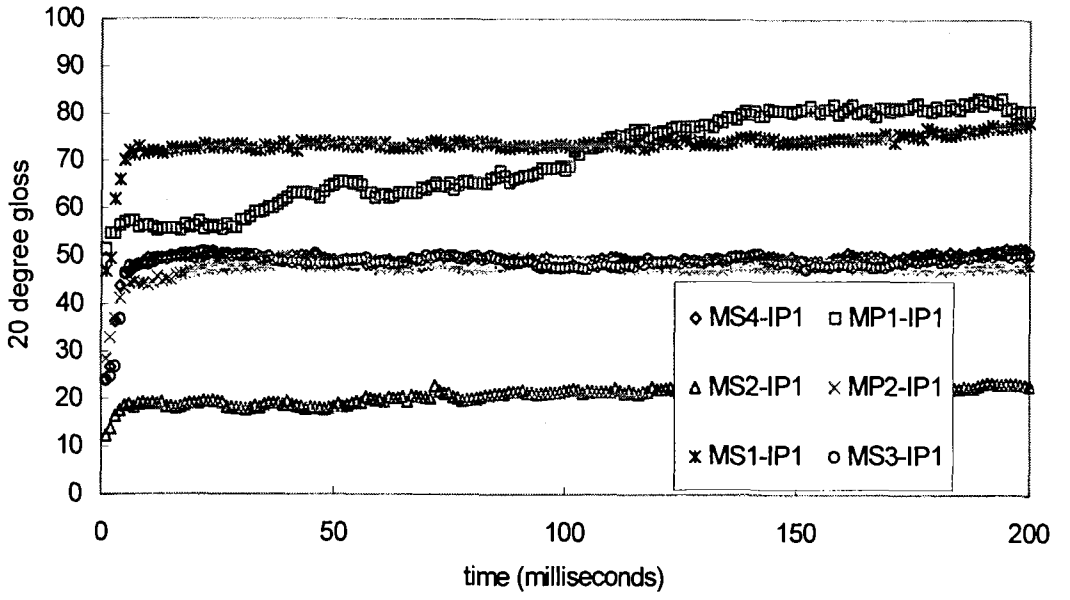

Figure 4.4 Short-time gloss developments with ink IP1

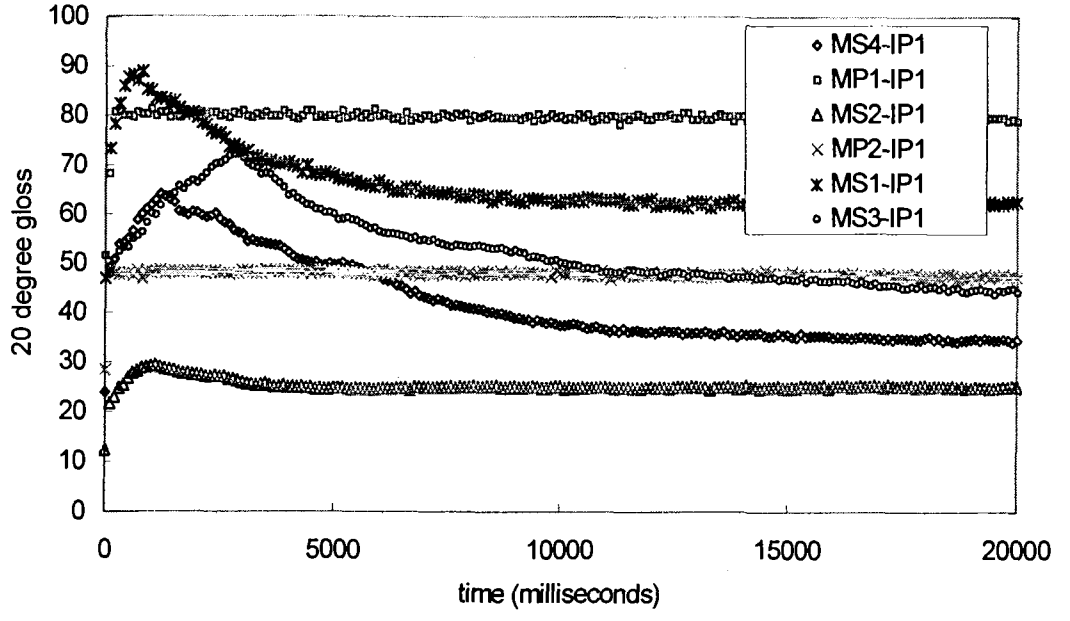

Figure 4.5 Long-term gloss developments with ink IP1

Table 4.3 Standard deviation data for ink IP1 (gloss)

	MS1	MS2	MS3	MS4	MP1	MP2
Min. std.dev.	2.20	9.92	1.69	0.95	2.84	1.60
Max. std.dev.	13.07	21.40	33.12	19.52	7.36	5.02
Avg. std.dev.	5.31	16.03	16.45	6.83	5.51	3.26

As can be seen in Figure 4.6, the gloss rises to its high value in less than 10 ms. Figure 4.7 shows the complete results, measured up to 20 s. The porous media can be seen to reach their final gloss rapidly, while the swellable media seem to reach a maximum near 6 seconds, followed by a gradual decrease to a final plateau. The trends observed for the final gloss values at 20 s seem to correlate with the water absorption trends, except for MS2, which shows a high level of coating dissolution in water. A probable explanation could be that the gloss of the liquid layer controls the gloss till the time scale of interest. The ink IP2 does not seem to possess many water-like properties except for the lowest value of filtercake resistance. The diffuse peaks in the gloss could be due to the maximum leveling of the film, after which the media roughening and absorption takes over; however the ink film above the pigment layer still seems to control the gloss in this region.

The gloss results for ink IP1 are qualitatively similar to those of ink IP2 in the gradual rise, and the final leveling out. The gloss of the swellable media drops during drying except for MS1, which is the least swellable medium, as can be seen in Table 4.2. Since IP2 has the highest pigment size, the decrease in gloss indicates the combined effect of the wet roughness and pigment size on the final gloss. In

the case of MS1, due to its low-swelling characteristics, the final gloss seems to be unaffected by the wet roughness and is dependent on the dry unprinted media gloss.

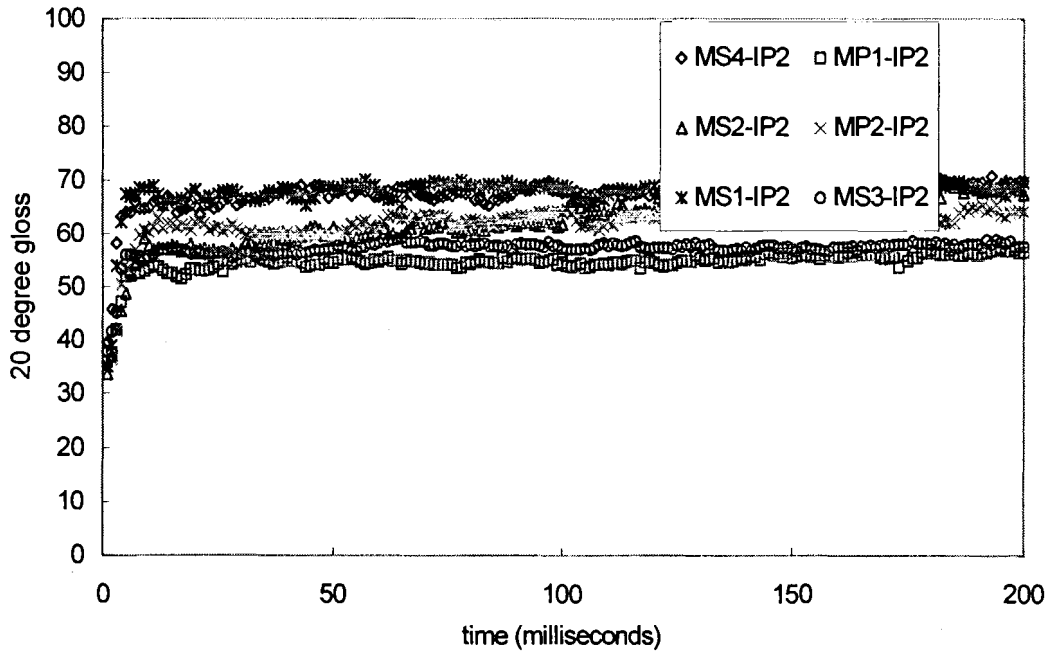

Figure 4.6 Short-time gloss developments with ink IP2

Table 4.4 Standard deviation data for ink IP2 (gloss)

	MS1	MS2	MS3	MS4	MP1	MP2
Min. std.dev.	6.39	1.63	7.80	1.72	3.45	6.17
Max. std.dev.	19.42	23.53	31.23	15.14	11.11	14.71
Avg. std.dev.	15.90	19.02	18.54	5.93	5.74	13.35

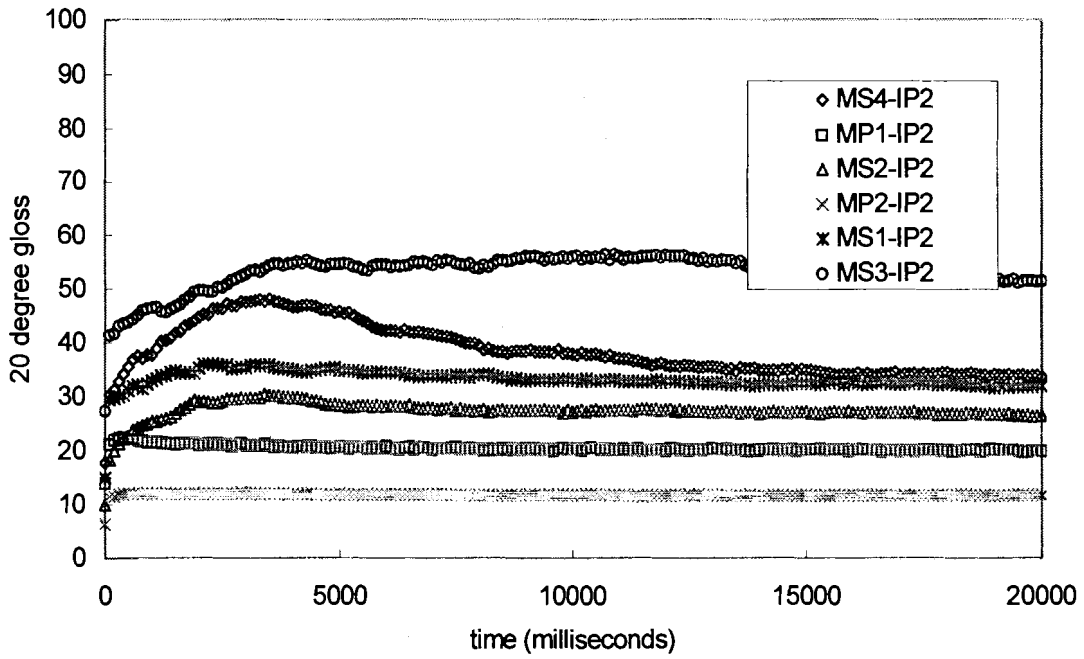

Figure 4.7 Long-term gloss development with ink IP2

The gloss of ink IP3 differs from that of the other pigmented inks in that very small peaks are observed in the initial region as shown in Figs. 4.8 and 4.9. In this respect IP3 behaves like a dye-based ink without pigments. IP3 also has the smallest pigment size, and the reason the porous media show higher gloss than the swellable ones could be that the small pigments conform to the roughness of the wet roughness of the swellable media instead of masking it. Another observation is that IP3 uniformly increases the final dry gloss with all media, irrespective of type, as seen in Table 4.2 IP3 has the lowest surface tension, relatively high solids content, and the highest viscosity. The added effects of viscosity and surface

tension in the leveling constant β imply the highest leveling time, but the leveling time does not seem to be a big issue.

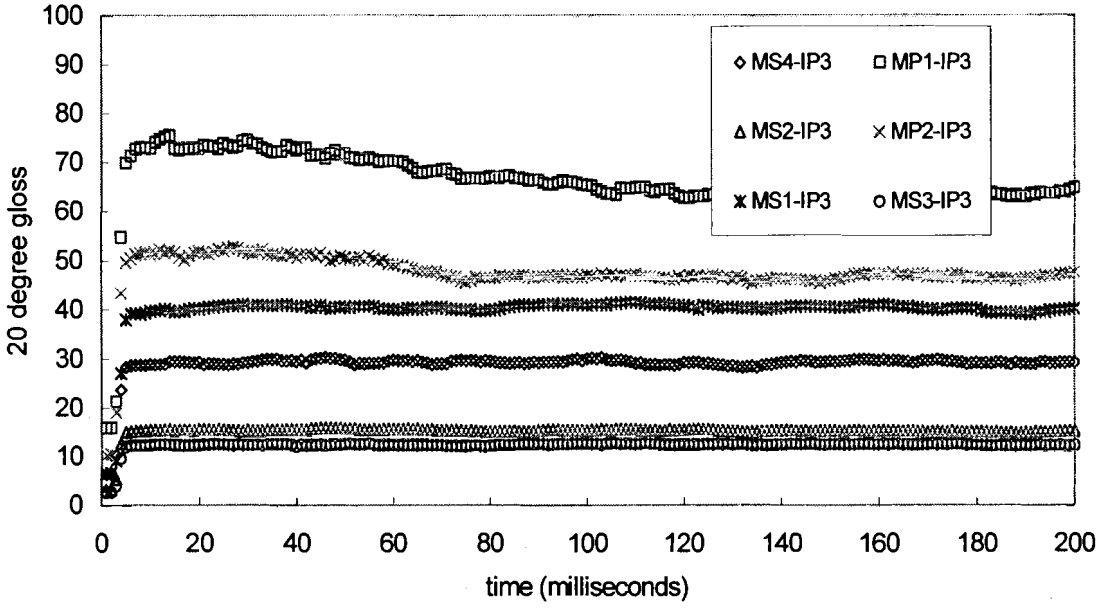

Figure 4.8 Short-time gloss development with ink IP3

Table 4.5 Standard deviation data for ink IP3 (gloss)

	MS1	MS2	MS3	MS4	MP1	MP2
Min. std.dev.	1.68	1.75	3.66	4.52	4.10	0.75
Max. std.dev.	6.19	12.23	10.68	10.29	9.53	6.58
Avg. std.dev.	3.57	3.57	6.46	8.48	7.75	3.56

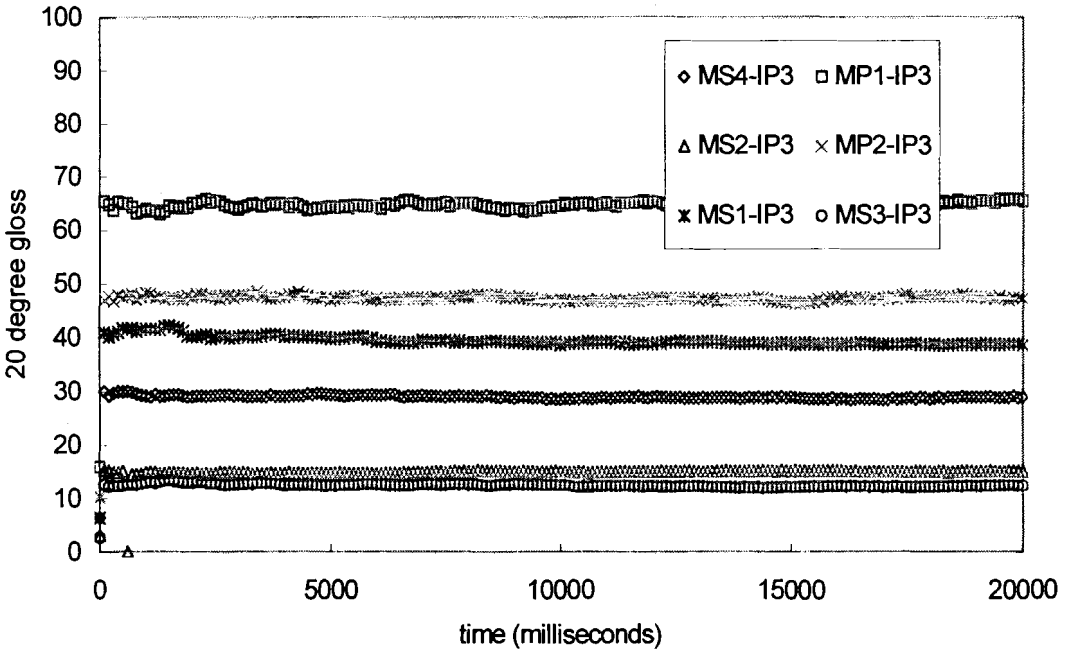

Figure 4.9 Long-time gloss development with ink IP3

The media gloss seems to be the controlling element for the dye-based ink ID1. Also, no peaks are seen, and a final value is reached almost instantaneously. ID1 differentiates between the porous and swellable media in that the print gloss of the porous media is quite close to the unprinted gloss. This is expected since the dye molecules are much smaller than the pigments, and do not influence the roughness of the porous media. The gloss of the swellable media is strongly dependent on the swelling roughness when wet because the gloss even after 24 hours is much lower than the unprinted gloss.

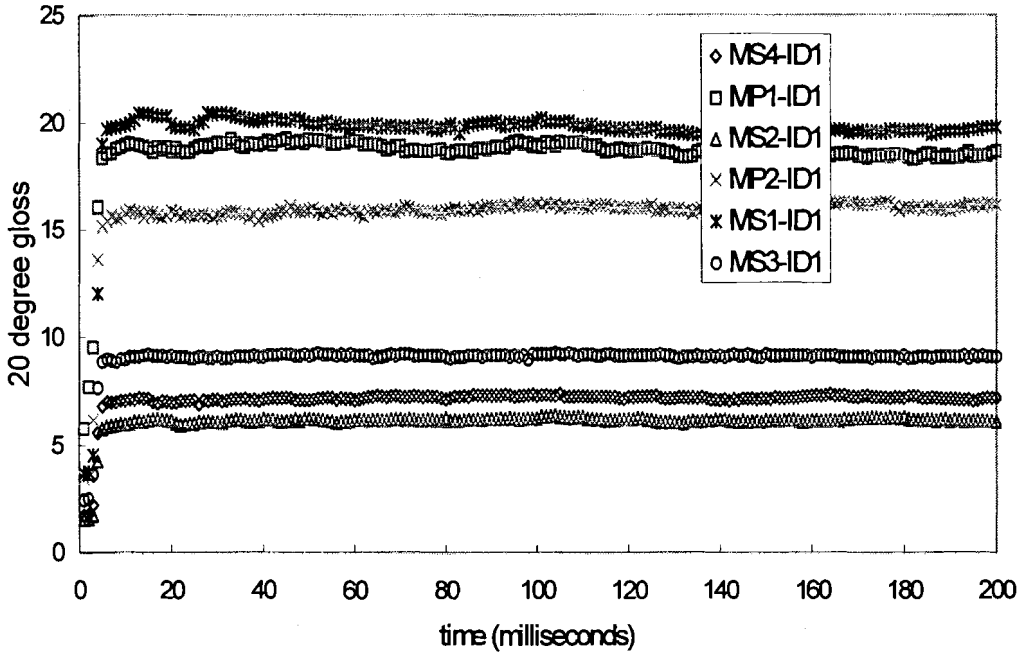

Figure 4.10 Short-time gloss development for dye-based ink ID1

Table 4.6 Standard deviation data for ink ID1 (gloss)

	MS1	MS2	MS3	MS4	MP1	MP2
Min. std.dev.	2.02	1.57	8.64	6.23	6.38	0.44
Max. std.dev.	12.27	16.72	19.53	14.72	24.78	4.08
Avg. std.dev.	4.50	3.99	10.00	7.68	8.91	1.97

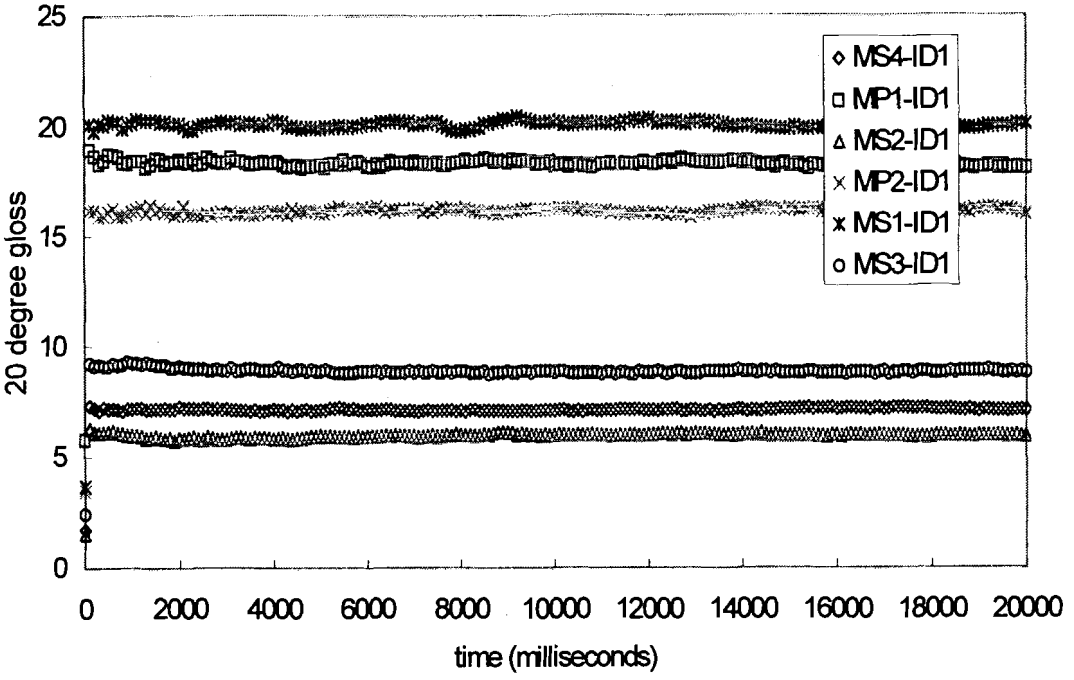

Figure 4.11 Long-time gloss development for ink ID1

The results for the other dye-based ink ID2 can be seen in Figure 4.12

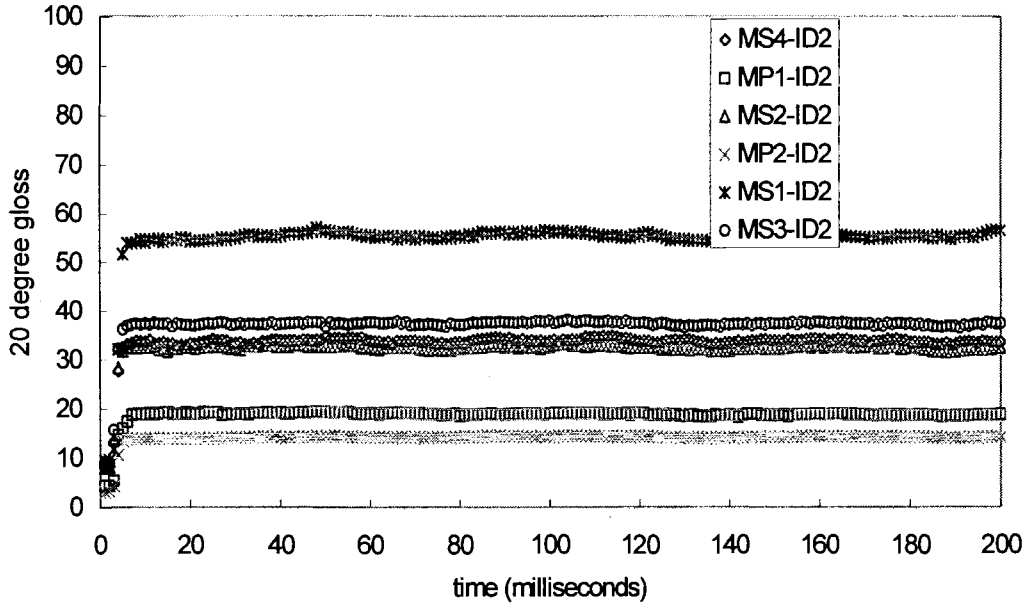

Figure 4.12 Short-time gloss results for dye-based ink ID2

Table 4.7 Standard deviation data for ink ID2 (gloss)

	MS1	MS2	MS3	MS4	MP1	MP2
Min. std.dev.	0.59	0.50	1.36	1.41	0.79	0.00
Max. std.dev.	3.20	4.38	3.86	6.34	4.43	5.73
Avg. std.dev.	1.82	1.97	2.53	4.07	2.33	3.05

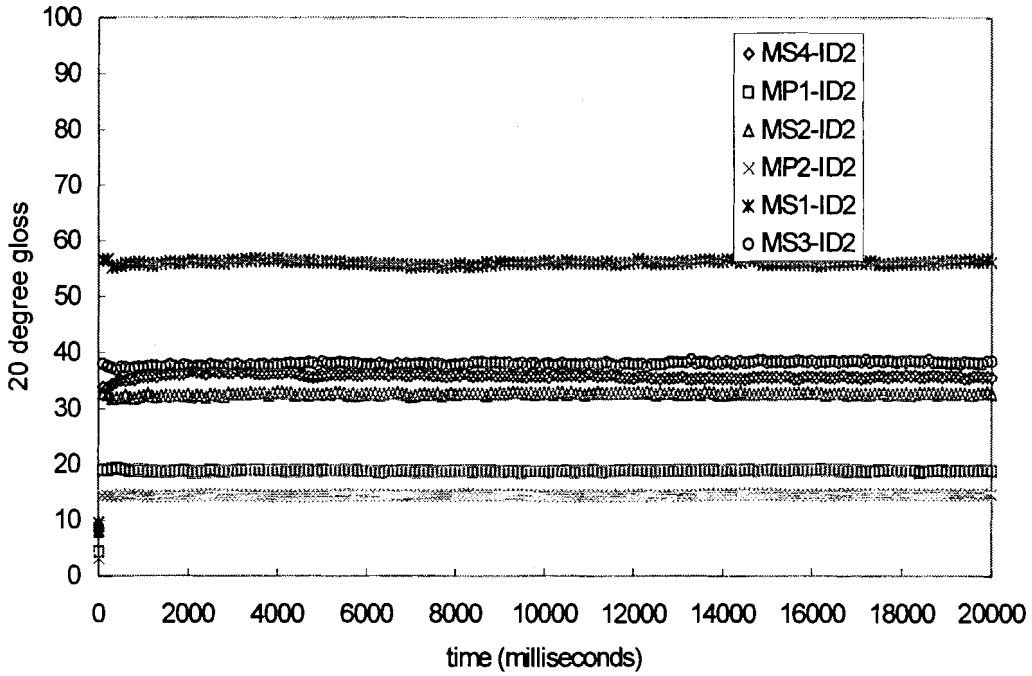

Figure 4.13 Long-time gloss development with ID2

ID2 displays similar gloss behavior as ID1 with the porous media, with the printed gloss being close to the unprinted media gloss for upto 24 hours. ID2 has a lower viscosity and a lower surface tension than ID1, however this does not seem to affect the gloss in the 20-second regime qualitatively, when compared with the behavior of ID1. A significant difference between the two dye inks is that with ID2, the gloss approaches closer to the unprinted media gloss for the swellable media in the 24-hour period.

4.4 Comparison with model predictions

The gloss predicted by the model, based on pigment size, wet roughness, and the leveling rates is compared with the experimental data in this section. The values of some of the parameters used in the model are given in Table 4.7.

Table 4.8 Assumed values for the model parameters

Media	ε (void fraction)	K (Darcy constant m^2)	r_p (pore radius in microns)	D (diffusion coefficient m^2/s)
MP1	0.35	$0.55*10^{-18}$	0.015	----
MP2	0.39	$0.90*10^{-18}$	0.021	----
MS1	----	-----	-----	$5.0*10^{-11}$
MS2	----	----	-----	$5.2*10^{-11}$
MS4	----	-----	-----	$5.0*10^{-11}$
MS3	----	------	-------	$4.5*10^{-11}$

The Darcy constants were calculated using the Bristow absorption data. If Eq. (3.22) is written in terms of volume absorbed per area "V", the ink and filtercake mass balances change as

$$h_s = \frac{V}{\varepsilon} \tag{4.2}$$

and

$$h_f = \frac{V\phi}{\phi_m} \tag{4.3}$$

Substituting h_s from Eq. (4.2) in Eq. (3.10) alongwith Eq. (3.22) gives

$$\frac{dV}{dt} = \frac{2\gamma \cdot \cos(\theta)/R_p}{\mu \cdot \left[\frac{V\phi}{\phi_m K_f} + \frac{V}{\varepsilon K_s}\right]} \tag{4.4}$$

Integrating Eq. (4.4) gives

$$V = \sqrt{\frac{4t\,\gamma \cdot \cos(\theta)/R_p}{\mu \cdot \left[\frac{\phi}{\phi_m K_f} + \frac{1}{\varepsilon K_s}\right]}} \tag{4.5}$$

The value of K_s is not known but is adjusted to match the Bristow wheel results. The diffusion coefficient for the swellable media is found by matching the Bristow wheel results.

Figures (4.14-4.27) show the show the experimental and theoretical curves for several combinations. The gloss calculation scheme shown in Figure 4.2 was used for the model calculations.

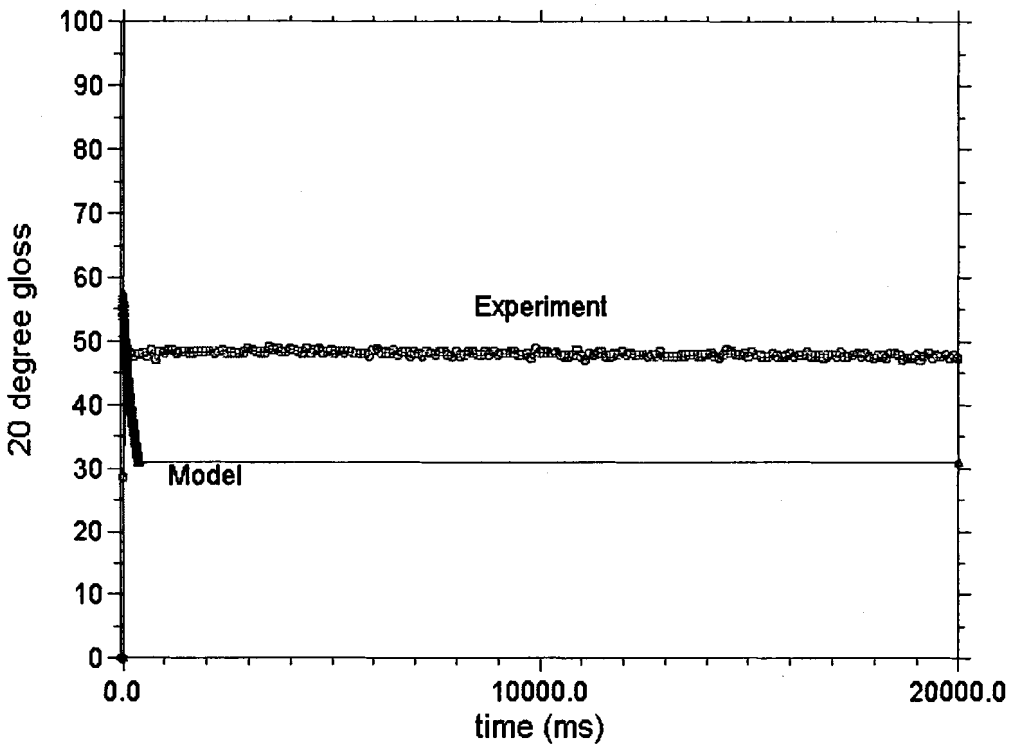

Figure 4.14 Model and experimental gloss for IP1-MP1

The model overpredicts the rise for the combination IP1-MP1, IP1-MP2 and underpredicts the gloss. A possibility is that the IP1 pigments smooth out the surface roughness, giving rise to a higher gloss than expected. The model predicts a lower gloss for the porous media MP2. Another reason could be that the laser beam penetrates the ink layer and reflects off the ink-media interface, thus adding to the overall gloss. The model predicts a rapid decrease in gloss for the swellable media. The combination IP1-MS1 shows a much higher experimental value, which could probably be ascribed to the low water-absorption capacity, but good spreading behavior of MS1 (low contact angle with water), which could mean

good leveling without rapid absorption. Also, MS1 does not exhibit significant swelling effects.

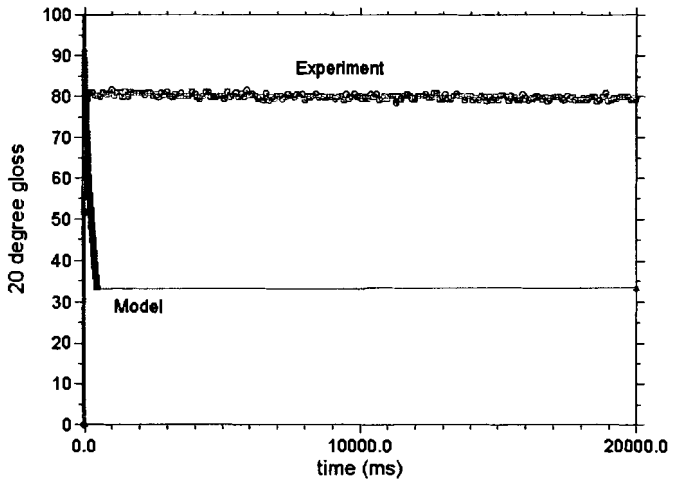

Figure 4.15 Model and experimental gloss for IP1-MP2

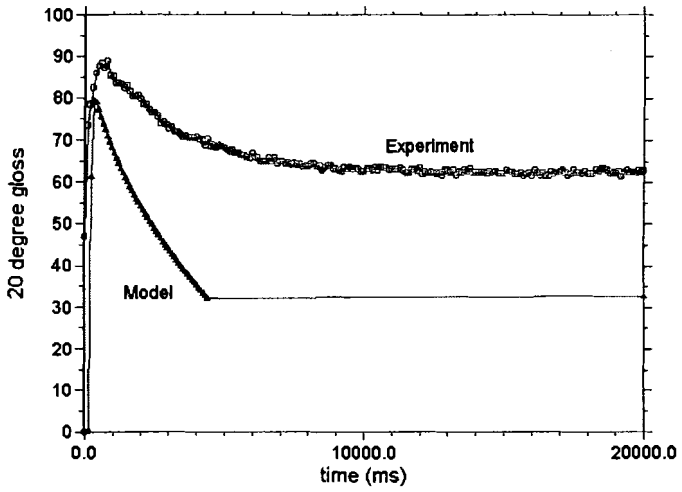

Figure 4.16 Model and experimental gloss for IP1-MS1

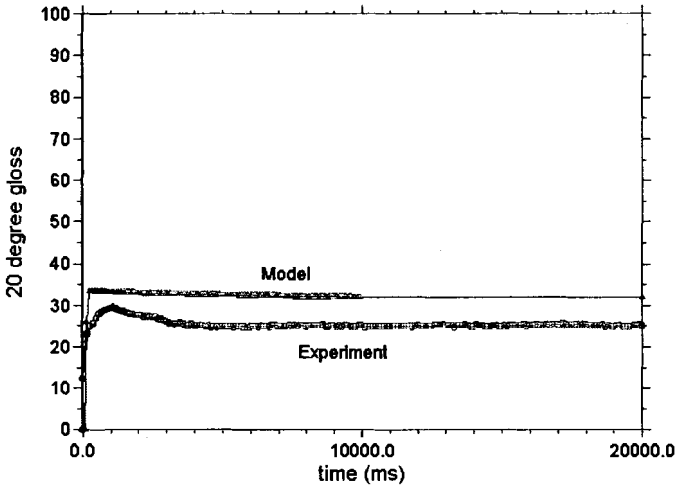

Figure 4.17 Model and experimental gloss for IP1-MS2

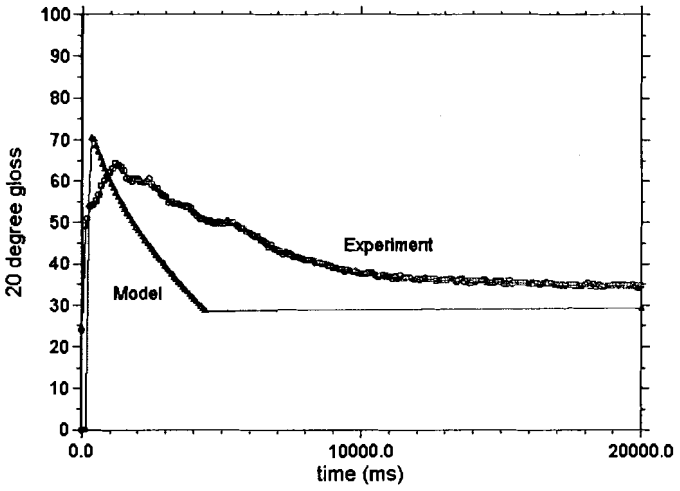

Figure 4.18 Model and experimental gloss for IP1-MS4

The gloss of the porous media with dye-based ink is similar to the dry media gloss as shown in Figs. 4.19 and 4.20. This result indicates that the dye-

gloss is not a significant controlling factor for this combination. The model matches the experiments in that the gloss rapidly increases to the wet media gloss.

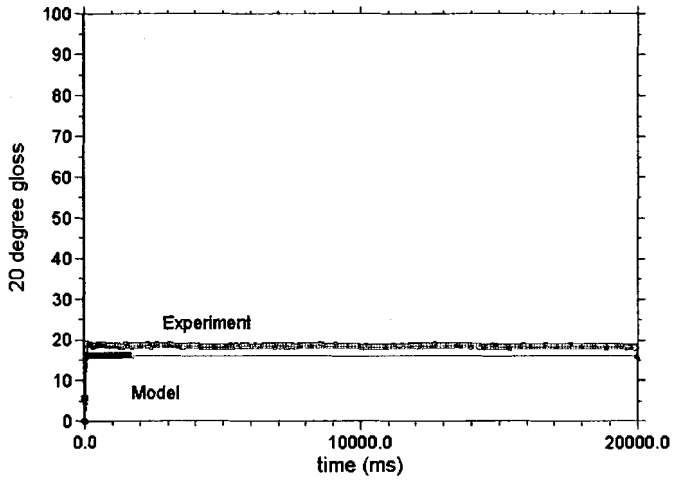

Figure 4.19 Model and experimental gloss for ID1-MP1

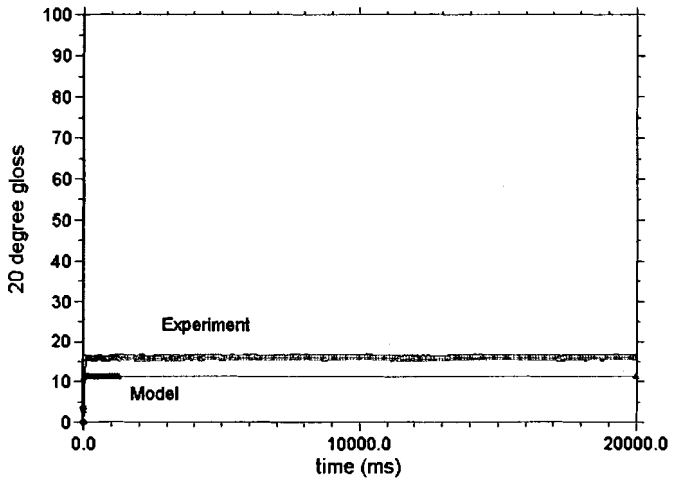

Figure 4.20 Model and experimental gloss for ID1-MP2

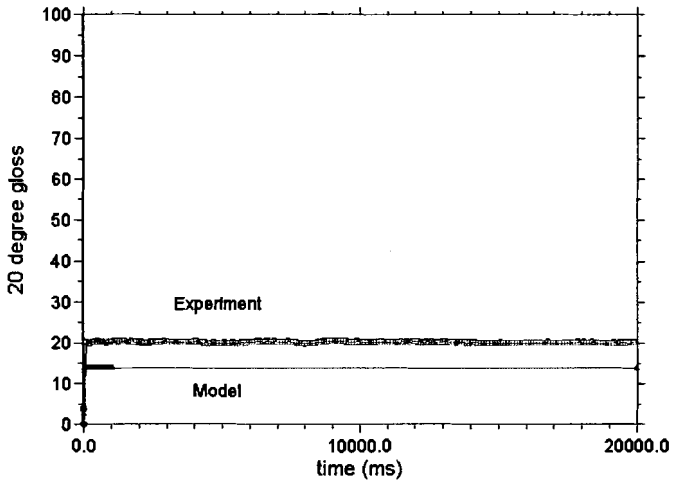

Figure 4.21 Model and experimental gloss for ID1-MS1

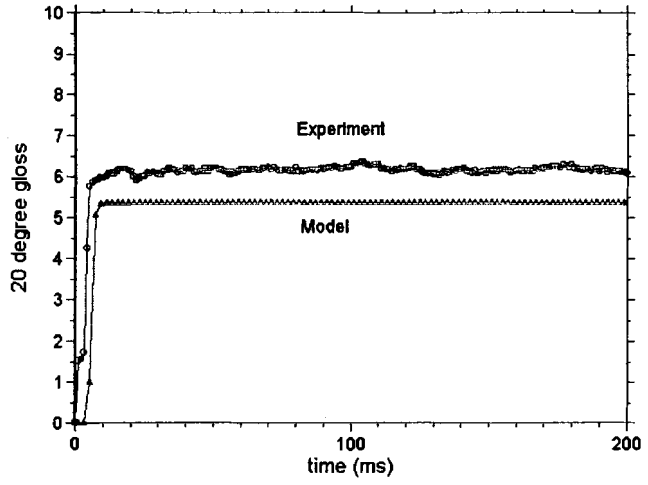

Figure 4.22 Short-time model and experimental gloss for ID1-MS2

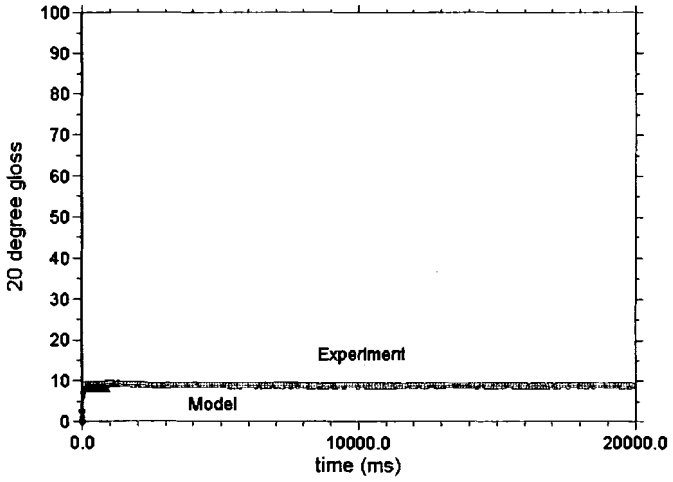

Figure 4.23 Model and experimental gloss for ID1-MS3

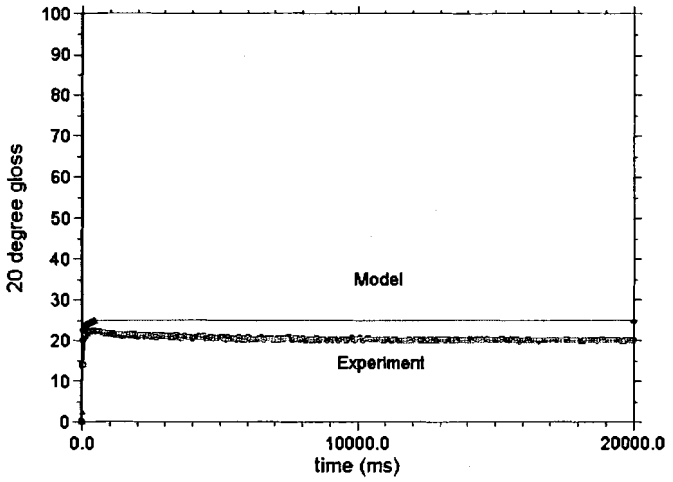

Figure 4.24 Model and experimental gloss for IP2-MP1

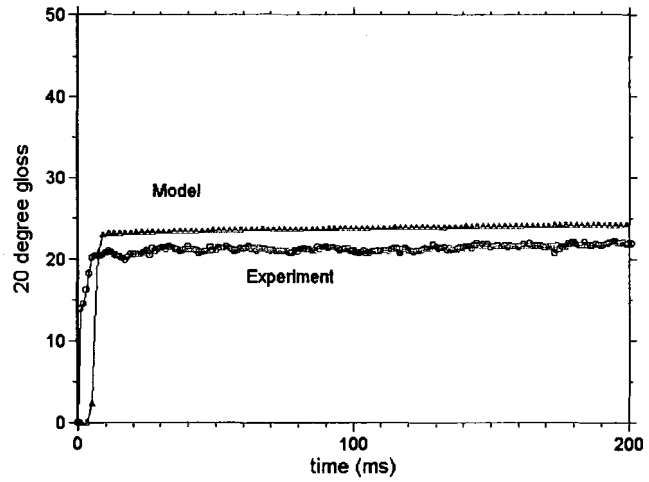

Figure 4.25 Short-time model and experimental gloss for IP2-MP1

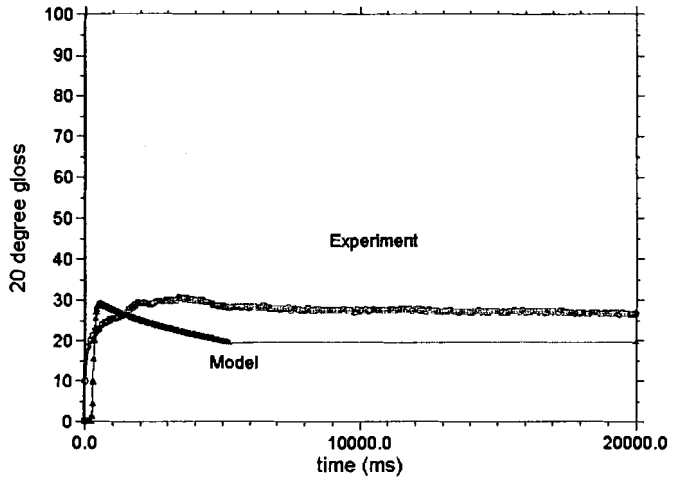

Figure 4.26 Model and experimental gloss for IP2-MS2

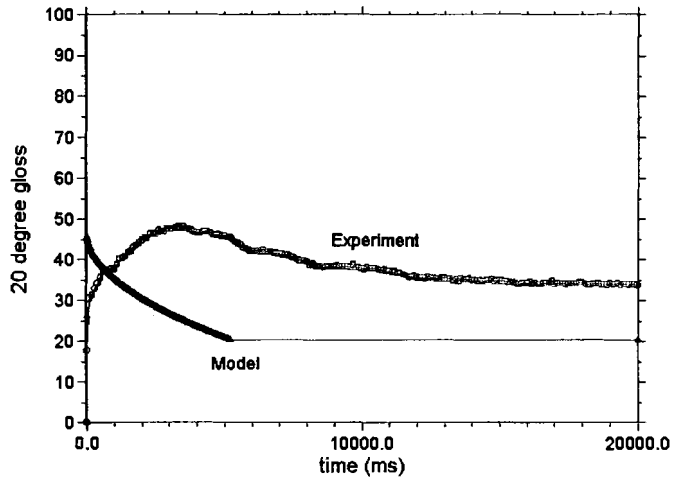

Figure 4.27 Model and experimental gloss for IP2-MS4

The media MS4 shows a relatively hydrophobic character with a high static contact angle with water. This may mean a localized smooth ink layer, or menisci formed within the polymer-ink matrix, which gives a slower drop in gloss due to slow absorption, and a higher gloss than expected. The slow drop in gloss is hard to understand. The Bristow absorption coefficient K_a for MS4-IP2 is 8.3 $cm^3m^{-2}t^{-1/2}$ indicating slow absorption. At 10 seconds, this would absorb around 24 cm^3m^{-2}, which is more than enough for a drop of ink. Figure 4.28 shows a comparison of the predicted and measured gloss for all the ink-media combinations. Apart from a few outliers, the model predicts the gloss with a reasonable amount of accuracy. The key outliers have been already discussed in the experimental gloss figures.

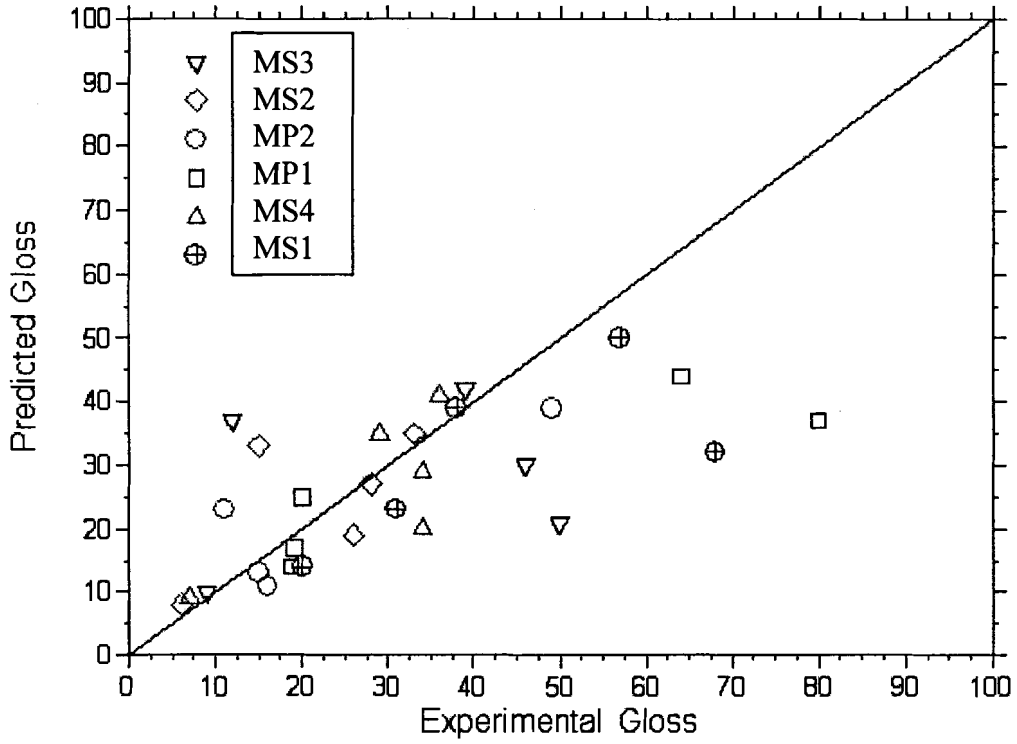

Figure 4.28 Experimental and predicted gloss

The observation of the gloss behavior of the dye-inks shows the inability of the dyes to affect the overall gloss as expected due to their molecular size, and the media gloss emerges as the primary element for the dye-porous media combinations, while the wet roughness seems to control the dye-swellable media combinations.

A case-wise study of specific ink-media combinations leads to some interesting observations. The final gloss of media MP1 with the pigmented inks shows that the lower the solids content of the ink, the higher is the final gloss at

20s. For the media MP2, a similar trend is seen except that a solids content of around 15% seems to be the maximum value, below which a high gloss is observed. This is deduced from the fact that the ink IP3, which has a solids content of about 15%, but the smallest pigment size, behaves like a dye-based ink with respect to gloss.

4.5 Conclusions

The model seems to predict the qualitative rise and decrease in gloss for swellable media with pigmented inks with some accuracy. The experiments and the model agree in the four main combinations:

1) The gloss of dye-based inks on porous media is controlled by media roughness.
2) The gloss of dye-based inks on swellable media is determined by the wet media roughness.
3) The gloss of pigmented inks on porous media is determined by a combination of ink pigment size and media smoothness.
4) The gloss of pigmented inks on swellable media is determined by a combination of pigment size and wet media roughness.
5) In most cases, the gloss is determined by the events occurring within 30 ms.
6) Due to the rapid leveling process, a higher degree of absorption could be used without affecting the leveling dynamics.

The final gloss on the porous media not much different than that right after printing, but swellable media gloss after complete drying is often higher than the

wet gloss due to the consolidation of the polymer coating due to loss of the water by evaporation and absorption.

The model could be improved with a further understanding of the polymer swelling process and the experiments with coatings with known properties should help isolate the effects of the various properties such as coating weight, pore size distribution, diffusion rate on the gloss development. Further experiments to ascertain and isolate the effect of laser transmittance through the coating, could improve the calculations.

References

Adamson, A.W. (1967). Physical Chemistry of Surfaces. Interscience publishers, 353. [12]

Agbezuge, L., and Carreira, L.M. (1998). Ink/Media Interactions in Ink Jet Printing-Tutorial notes. IS&Ts NIP 14: International Conference on Digital Printing Technologies. [16]

Arai Y., and Nojima K., (1998). Coating structure for obtaining high print gloss. TAPPI J. 81(5), 213. [21]

Asbeck W.K., and van Loo, M., (1949). Critical pigment volume relationships. Industrial and Engineering Chemistry, 41(7), 1470. [9]

Aspler J.S., and LePoutre P., (1991). The transfer and setting of ink on coated paper. Progress in Organic Coatings, 10, 333. [18]

Beland M.-C., and Bennett J.M., (2000). Effect of local microroughness on the gloss uniformity of printed paper surfaces. Applied Optics, 39(16), 2719. [22]

Bird, R.B., Stewart, W.E., and Lightfoot, E.N., (1960). Transport Phenomena. Wiley, New York. [35]

Bristow J.A., (1967). Liquid Absorption into Paper during Short Contact Time Intervals. Svenk Papper Stidning,70(19), 623. [32]

Carreira, L., Agbezuge, L., and Gooray, A., (1996). Correlation between drying time and ink jet print quality parameters. Recent Progress in Ink-Jet Technologies, Rezanka, I., and Eschbach, R., (Eds.) Society for Imaging Science and Technology, 215. [5]

Chapman, D.M., and Michos, D., (1999). Novel sub-micron silica gels for glossy ink-receptive coatings. IS&T's NIP 15: 1999 International Conference on Digital Printing Technologies, 164. [1]

Chinmayanandam T.K., (1919). On the Specular Reflection From Rough Surfaces. Phys.Rev.,13(2), J96 [28]

Desjumaux, D.M., (1999). The Influence of Coating and Ink Properties on Ink Setting Rate on Coated Paper. Ph.D. Thesis, University of Maine.

Desjumaux D., and Bousfield D.W., (1998). Modeling of ink film leveling with mobile phase removal. Proc. Pan-Pacific and International Printing and Graphic Arts Conference Oct 6-8, 103. [33]

Donigian D.W., Ishley J.N., and Wise K.J., (1997). Coating Pore Structure and Offset Printed Gloss. TAPPI J., 80, 163. [20]

Glatter T., and Bousfield D.W., (1997). Print gloss development on a model substrate. TAPPI J., 80(7), 125. [19]

Gregory, P. (1996). Dyes versus pigments: The truth. Recent Progress in Ink-Jet Technologies, Rezanka, I., and Eschbach, R., Eds. Society for Imaging Science and Technology, 276. [6]

Halko, D.J. (1996). Kogation: A New Mechanism and Solution, Recent Progress in Ink-Jet Technologies, Rezanka, I., and Eschbach, R., Eds. Society for Imaging Science and Technology, 215. [3]

Hiemenz, P., and Rajagopalan, R., (1997). Principles of Colloid and Surface Chemistry. Marcel Dekker. [13]

Kasahara, K. (1999). A new quick-drying, high-water-resistant glossy ink jet

paper. Recent Progress in Ink Jet Technologies II, Hanson, E., Ed. Society for Imaging Science and Technology, 353. [9]

KSV Sigma 70 Instruction Manual, KSV Instruments USA, PO Box 192, CT 06468 [29].

Le, H.P., (1999). Progress and trends in ink-jet printing technology. Recent Progress in Ink Jet Technologies II, Hanson, E., Ed., Society for Imaging Science and Technology, 1. [7]

Lee, D.I., (1974). A Fundamental Study of Coating Gloss. Proc. 1974 Coating Conference, 97, TAPPI Press Atlanta. [24]

LePoutre P., and Rezanowich A., (1977). Optical properties and structure of clay-latex coatings. TAPPI J., 60(11), 86. [28]

Marmur, A., and Cohen, R., (1997). Characterization of porous media by the kinetics of liquid penetration: The vertical capillaries model. J. Colloid and Interface Sci., 189. 299 [17]

McCabe, W.L., Smith, J.L., and Harriott, P., (1985). Unit Operations of Chemical Engineering. McGraw-Hill. [31]

Middleman, S., (1995). Modeling Axisymmetric Flows. Academic Press. [10]

Neumann, A.W., and Spelt, J.K., (1996). Applied Surface Thermodynamics. Marcel Dekker. [15]

Oittinen, P., and Saarelma, H., Eds. (1998). Printing, Book 13. TAPPI Press, Fapet Oy, PO Box 146, FIN-0071 Helsinki, Finland. [2]

Oliver, J.F., (1984). Initial stages of ink drop impaction, spreading, and wetting on paper. TAPPI J., 60, 90. [11]

Poresizer 9320 Manual, Micomeritics, Norcross, GA 30093-1877 U.S.A. [30]

Ryu, R.Y., Gilbert, R.D., and Khan, S.A. (1999). Influence of cationic additives on the rheological, optical, and printing properties of ink-jet coatings. TAPPI J., 82(11), 128. [4]

Sakai, H., and Fujii, T., (1999). The dependence of the apparent contact angles on gravity. J. Colloid and Interface Sci., 210, 152. [14]

Steiger, R., and Brugger, P.-A., (1998). Photochemical studies on the lightfastness of ink-jet systems. IS&Ts NIP 14: International Conference on Digital Printing Technologies, 114. [8]

Stover, J.C., (1990). Optical Scattering –Measurement and Analysis. McGraw-Hill. [27]

User's Guide to AutoProbe M5, Park Scientific Instruments, CA 94089 U.S.A. [25]

User's Manual, Tencor Instruments, PO Box 3308, NH 03802, U.S.A. [26]

Appendix A

Filtercake Resistance Calculations

Ink: IP1

$\Delta P = 25.6 \times 10^{3}\ Nm^{-2}$

A (Area) = $8 \times 10^{-4}\ m^{2}$

$\mu = 0.86 \times 10^{-3}\ kg\ m^{-1}s^{-1}$

V (volume of filtrate) = $0.17 \times 10^{-6}\ m^{3}$

t (time of filtration) = 30 s

$$u = \frac{V}{At} \tag{A.1}$$

c (mass of solids/volume of filtrate) = $100.52\ kgm^{-3}$

m_c= Vc (Total solids in cake)

$m_c = 1.78 \times 10^{-5}$ kg

$$\alpha = \frac{\Delta P \cdot A}{\mu \cdot u \cdot m_c} \tag{A.2}$$

$\alpha = 1.2 \times 10^{15}\ m\ kg^{-1}$

Graphical method:

K_c(slope of t/V vs V) = (2) (8 x 10^{14})

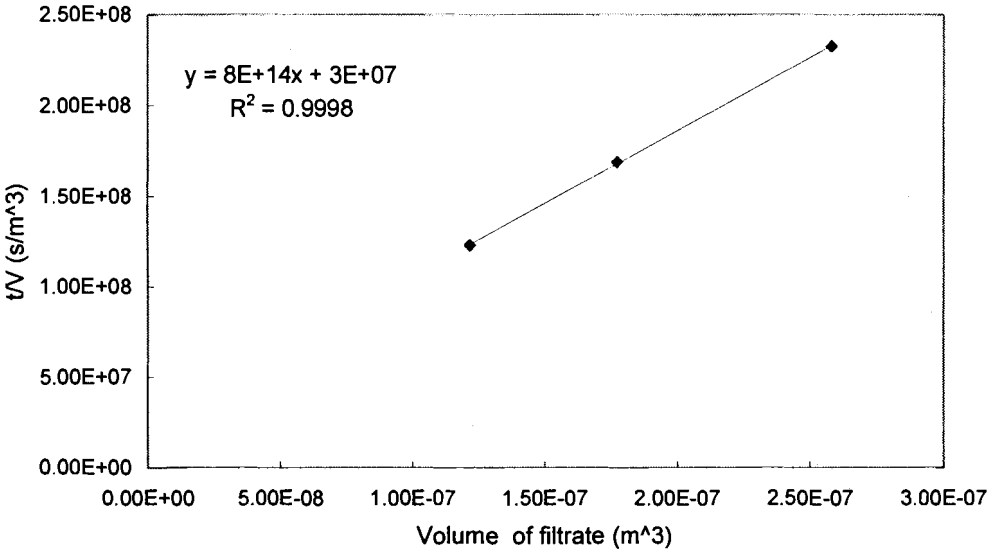

Figure A.1 Graph of t/V vs V for IP1 1

$$\alpha = \frac{A^2 \cdot \Delta P \cdot K_c}{\mu \cdot c} \qquad (A.3)$$

$\alpha = 2.0 \times 10^{15}$ m kg^{-1}

Ink: IP2

$\Delta P = 25.6 \times 10^3$ Nm^{-2}

A (Area) = 8×10^{-4} m^2

$\mu = 0.86 \times 10^{-3}$ kg m^{-1}s^{-1}

V (volume of filtrate) = 0.12×10^{-6} m^3

t (time of filtration) = 30 s

c (mass of solids/volume of filtrate) = 257.14 kgm^{-3}

$m_c = 3.11 \times 10^{-5}$ kg

$\alpha = 1.02 \times 10^{15}$ m kg^{-1}

Graphical method:

K_c(slope of t/V vs V) = (2) (2×10^{15})

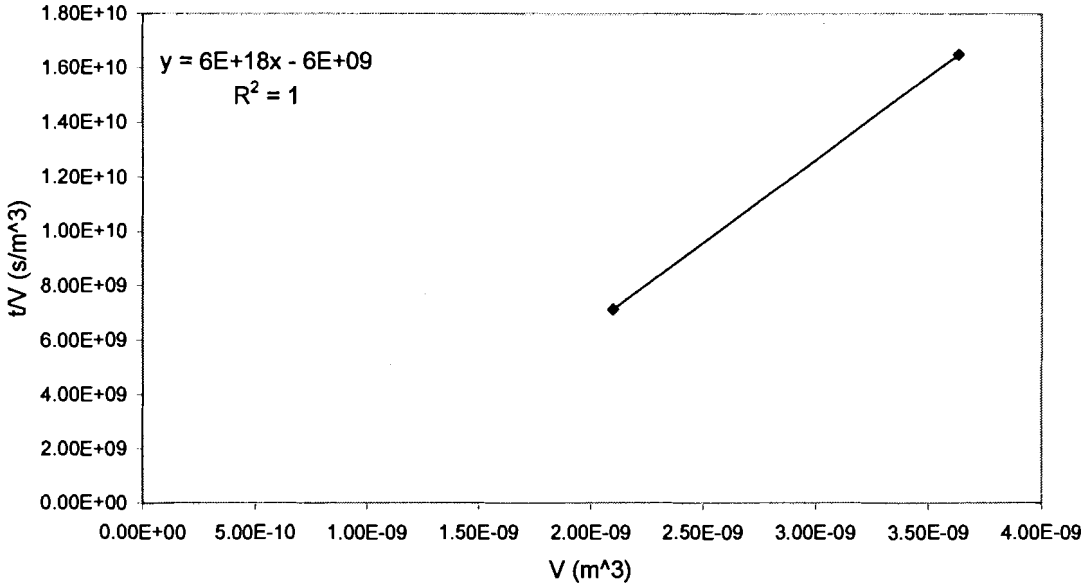

Figure A.2 Graph of t/V vs V for IP2 1

$\alpha = 1.9 \times 10^{15}$ m kg^{-1}

Ink: IP3

$\Delta P = 25.6 \times 10^{3}$ Nm^{-2}

A (Area) = 8×10^{-4} m^2

$\mu = 0.86 \times 10^{-3}$ kg m^{-1}s^{-1}

V (volume of filtrate) = 0.09×10^{-6} m^3

t (time of filtration) = 30 s

c (mass of solids/volume of filtrate) = 186.04 kgm^{-3}

$m_c = 1.80 \times 10^{-5}$ kg

$\alpha = 2.1 \times 10^{15}$ m kg^{-1}

Graphical method:

K_c(slope of t/V vs V) = (2) (3×10^{15})

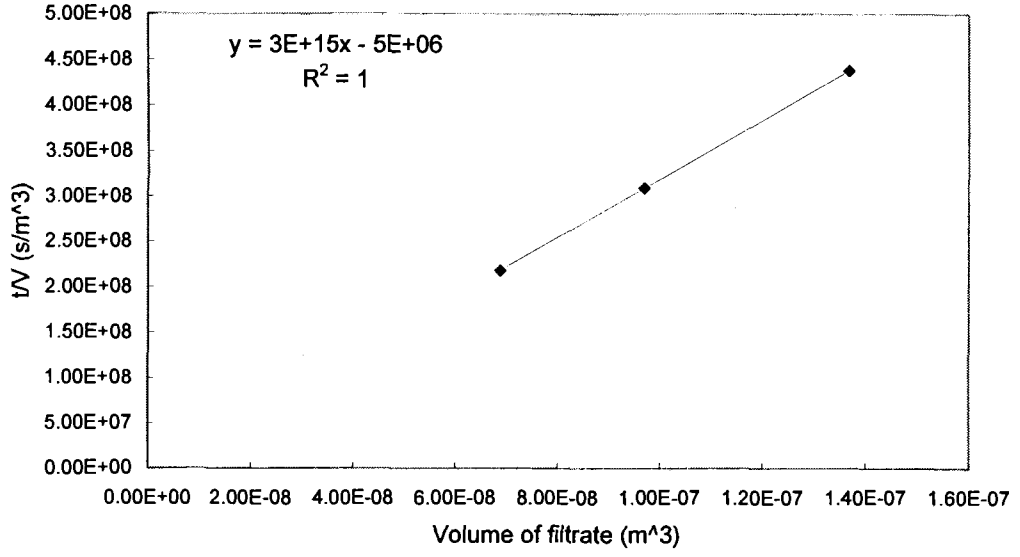

Figure A.3 Graph of t/V vs V for IP3

$\alpha = 4.1 \times 10^{15}$ m kg^{-1}

Appendix B

Visual Basic Data Acquisition Code

```
---------------------------------------------------------------------------------

'   PrintTest – Author: Prof. John C. Hassler, (The University of Maine)

' To use the printer control file, I had to

' read it in in BINARY, and then use the WIN32 API

' to bypass the printer driver.  The API methods are from

' Knowledge Base articles Q154078 and Q138594

' This version includes the ComputerBoards code.

---------------------------------------------------------------------------------

Option Explicit

' --- for the WIN32 API calls ----\

' raw print spool API

Private Type DOCINFO

  pDocName As String

  pOutputFile As String

  pDatatype As String

End Type

Private Declare Function ClosePrinter Lib "winspool.drv" (ByVal _

    hPrinter As Long) As Long

Private Declare Function EndDocPrinter Lib "winspool.drv" (ByVal _

    hPrinter As Long) As Long

Private Declare Function EndPagePrinter Lib "winspool.drv" (ByVal _
```

```
    hPrinter As Long) As Long
Private Declare Function OpenPrinter Lib "winspool.drv" Alias _
    "OpenPrinterA" (ByVal pPrinterName As String, phPrinter As Long, _
    ByVal pDefault As Long) As Long
Private Declare Function StartDocPrinter Lib "winspool.drv" Alias _
    "StartDocPrinterA" (ByVal hPrinter As Long, ByVal Level As Long, _
    pDocInfo As DOCINFO) As Long
Private Declare Function StartPagePrinter Lib "winspool.drv" (ByVal _
    hPrinter As Long) As Long
Private Declare Function WritePrinter Lib "winspool.drv" (ByVal _
    hPrinter As Long, pBuf As Any, ByVal cdBuf As Long, _
    pcWritten As Long) As Long

' Performance counter API's
Private Declare Function QueryPerformanceCounter Lib "kernel32" _
        (lpPerformanceCount As Currency) As Long
Private Declare Function QueryPerformanceFrequency Lib "kernel32" _
        (lpFrequency As Currency) As Long
Private secFreq As Currency, secStart As Currency, secEnd1 As Currency
' --- end Winapi declares ---
' --- begin CB declares ---
Private ULStat As Integer
Private ChanNo As Integer, CBCount As Long
```

```
Const BoardNum As Integer = 0
Const CBRange As Integer = UNI10VOLTS
' --- end CB declares ---

' ******* set the rate and number of points here *******
Const Msec As Single = 1
Const NumPoints As Integer = 30000
' ************************************
Private InDat(NumPoints) As Integer
Private Ix As Integer
Private BinData(10000) As Byte, bTemp As Byte
Private Sub cmdExit_Click()
Unload Me
End
End Sub
-------------------------------------------------------------------------------------
Private Sub cmdFileOpen_Click()
Dim FName As String, TmpString As String, FilHandle As Integer
Dim i As Integer, j As Integer
With cdbFile
.InitDir = "C:\HP Printer Files\"
.ShowOpen
FName = .FileName
```

```
End With
If FName = "" Then
  txtShow.Text = "No file specified."
  Exit Sub
Else
  txtShow.Text = FName & vbCrLf
  FilHandle = FreeFile
' Must read file as binary since it has control char.
  Open FName For Binary As FilHandle
End If
Ix = 0
txtShow.Text = txtShow.Text & "Begin input loop." & vbCrLf

Do While Not EOF(FilHandle)
  Ix = Ix + 1
 Get #FilHandle, , BinData(Ix)  ' Binary, one byte at a time
 DoEvents
Loop
  txtShow.Text = txtShow.Text & "Finished reading." & vbCrLf
  txtShow.Text = txtShow.Text & "Number of bytes =" & Ix & vbCrLf
Close FilHandle
End Sub
```

```
Private Sub cmdPlot_Click()
' Collect and plot the data
picPlot.Cls
Dim MaxX As Integer, MaxY As Integer
MaxX = picPlot.ScaleWidth
MaxY = picPlot.ScaleHeight
Dim i As Integer, X As Integer, Y As Integer
Dim px(NumPoints) As Integer, py(NumPoints) As Integer
For i = 1 To NumPoints
  px(i) = (CSng(i) * MaxX / NumPoints)
  py(i) = (1 - InDat(i) / 4095) * MaxY
  picPlot.PSet (px(i), py(i))
  DoEvents
Next i
End Sub
```

```
Private Sub cmdPrint_Click()
 Dim i As Integer
 Dim lhPrinter As Long
 Dim lReturn As Long
 Dim lpcWritten As Long
 Dim lDoc As Long
 Dim sWrittenData As String
```

```
Dim MyDocInfo As DOCINFO
lReturn = OpenPrinter("HP DeskJet 970C Series", lhPrinter, 0)
If lReturn = 0 Then
 MsgBox "The Printer Name you typed wasn't recognized."
 Exit Sub
End If
 MyDocInfo.pDocName = "AAAAAA"
 MyDocInfo.pOutputFile = vbNullString
 MyDocInfo.pDatatype = vbNullString
 lDoc = StartDocPrinter(lhPrinter, 1, MyDocInfo)
 Call StartPagePrinter(lhPrinter)
 txtShow.Text = txtShow.Text & "Sending data to printer." & vbCrLf
 For i = 1 To Ix
  bTemp = BinData(i)  ' send one byte at a time by reference
  lReturn = WritePrinter(lhPrinter, bTemp, _
   Len(bTemp), lpcWritten)
 Next i

  lReturn = EndPagePrinter(lhPrinter)
  lReturn = EndDocPrinter(lhPrinter)
  lReturn = ClosePrinter(lhPrinter)
txtShow.Text = txtShow.Text & "Finished." & vbCrLf
  Call GetData
```

```
End Sub
---------------------------------------------------------------------------------
Sub GetData()
txtShow.Text = "Start Getdata." & vbCrLf
Screen.MousePointer = vbHourglass
DoEvents
CBCount = NumPoints
Dim i As Integer, Delta As Currency
' Uses Windows API call to the performance counter.
'  Appears to be good for sub-msec resolution.  This
'  gives a very accurate sampling at 1 msec.
Delta = Msec * secFreq / 1000
' wait until printer does something
Dim Temp1 As Integer, Temp2 As Integer
Temp2 = 0

ULStat = cbAIn(BoardNum, ChanNo, CBRange, Temp1)
Temp1 = Temp1 + 200
Do While Temp2 < Temp1
  ULStat = cbAIn(BoardNum, ChanNo, CBRange, Temp2)
Loop

' now collect data
```

```
 QueryPerformanceCounter secStart
 secEnd1 = secStart + Delta

For i = 1 To CBCount
 ULStat = cbAIn(BoardNum, ChanNo, CBRange, InDat(i))
 Do
  QueryPerformanceCounter secStart
 Loop Until secStart > secEnd1
 secEnd1 = secEnd1 + Delta
Next i
txtShow.Text = txtShow.Text & "End Getdata." & vbCrLf
DoEvents
Screen.MousePointer = vbDefault
End Sub
```

```
Private Sub cmdSave_Click()
Dim FName As String, TmpString As String, FilHandle As Integer
Dim i As Integer, j As Integer
AutoRedraw = True
With cdbFile
.InitDir = "\\Grad01\PSSP\amol\Project\gloss\newprinter"
.ShowSave
```

```
FName = .FileName
End With
If FName = "" Then
  txtShow.Text = "No file specified."
  Exit Sub
Else
  txtShow.Text = FName & vbCrLf
  FilHandle = FreeFile
  Open FName For Output As FilHandle
End If

For i = 1 To NumPoints
  Print #FilHandle, InDat(i)
Next i
txtShow.Text = txtShow.Text & "Finished saving." & vbCrLf

Close FilHandle
End Sub
--------------------------------------------------------------------------------
Private Sub Form_Load()
AutoRedraw = True
lblHeader.Caption = "HP Printer Test V. 1.10"
 ULStat = cbDeclareRevision(CURRENTREVNUM)
```

```
ULStat = cbErrHandling(PRINTALL, DONTSTOP)
  If ULStat <> 0 Then Stop

QueryPerformanceFrequency secFreq  ' frequency of timer

End Sub
```

Biography of the Author

Amol Shirke was born in Mumbai, India on September 14, 1973, where he was raised and received his primary and secondary education.

He enrolled at the Indian Institute of Technology, Mumbai in 1992 and obtained the degree of Bachelor of Technology in Chemical Engineering in 1996.

He served as a research engineer at the Indian Institute of Technology, Mumbai, in the Department of Chemical Engineering from 1996 to 1998.

He began his graduate study at the University of Maine in 1998. Amol is a candidate for the Master of Science degree in Chemical Engineering from The University of Maine in May, 2001.